Calculations of periodicity from Hα profiles of Proxima Centauri

Author:
John COLLINS

Supervised by:
Prof. H.R.A. JONES
Dr. J.R. BARNES

Centre for Astrophysics Research
School of Physics, Astronomy and Mathematics
University of Hertfordshire

Submitted to the University of Hertfordshire in partial fulfilment of the requirements of the degree of Master of Science by Research.

July 2016

Abstract

In this report the stellar rotation signal for Proxima Centauri is investigated. High-resolution spectra taken with UVES and HARPS of Proxima Centauri over a 13-year period is used as well as photometric observations of Proxima Centauri from ASAS and HST.

The Hα equivalent width and Hα index are measured (and found to be very similar), together with other measurements, skewness and kurtosis and a method that investigates the symmetry of the line, the Peak Ratio, is introduced which appears to return better results than the other measurements.

The investigations return a most significant period of 82.6 ± 0.1 days, confirming photometric results and ruling out a more recent result of 116.6 days which it is concluded is an artefact of the observation times.

It is also concluded that whilst spectroscopic Hα measurements can be used for period recovery, in the case of Proxima Centauri the available photometric measurements are more reliable. By using 2D models of Proxima Centauri to generate simulated Hα, it is found that reasonable distributions of plage and chromospheric features are able to reproduce the equivalent width variations in observed data and recover the rotation period. The period recovery is still effective after simulated noise and the effects of flares similar to those in the observed data the are added to the modelling results. However the 2D models used fail to generate the observed variety of line shapes measured by the peak ratio. It is concluded that only 3D models which incorporate vertical motions in the chromosphere can achieve this.

Declaration

I declare that no part of this work is being submitted concurrently for another award of the University or any other awarding body or institution. This thesis contains a substantial body of work that has not previously been submitted successfully for an award of the University or any other awarding body or institution.

Except where indicated otherwise in the submission, the submission is my own work and has not previously been submitted successfully for any award.

Acknowledgements

I gratefully acknowledge the advice and assistance of members of the Centre for Astrophysical Research at the University of Hertfordshire in the preparation of this report. I particularly want to thank my supervisors, Prof. H.R.A. Jones and Dr J. R. Barnes, at the University of Hertfordshire, (the latter now at the Open University) for their advice and assistance, particularly in bringing me up to speed in things I hadn't learnt properly (or at all) 4 decades ago.

The HARPS data was obtained from HARPS public database at the European Southern Observatory (ESO).

I also wish to thank Birgit Fuhrmeister and Lalitha Sairam for providing me with some additional data referred to in Fuhrmeister et al. (2011).

I acknowledge the value of the Vienna Atomic Line Database (VALD) for spectral line data and the ASAS for additional observations of Proxima Centauri.

All the figures were produced using MATPLOTLIB, which is associated with the SCIPY library (Jones et al., 2001).

Finally I must express my thanks to my wife, Sue Collins, for proof-reading and tolerating for most of the time my absence or distracted attention during the preparation of this report.

Contents

Abstract i

Acknowledgements iii

Contents iv

List of Figures vi

List of Tables x

List of Abbreviations xi

1 Introduction 1
- 1.1 The importance of the study of M-dwarf stars . . . 1
- 1.2 Activity and the rotation period . . . 2
- 1.3 The importance of Hα . . . 3
- 1.4 Proxima Centauri . . . 3
- 1.5 Methodology . . . 4

2 Periodicity from photometric measurements 5
- 2.1 ASAS . . . 5
- 2.2 HST . . . 10
- 2.3 Summary of photometric results . . . 12

3 Spectra of Proxima Centauri 13
- 3.1 HARPS and UVES spectra of Proxima Centauri . . . 14
- 3.2 Hα line measurements . . . 14
- 3.3 Flares in UVES data and X-ray values . . . 20
- 3.4 Possible flares on HARPS . . . 22
- 3.5 Recovery of periods from HARPS data . . . 24
- 3.6 Comparison of ASAS and HARPS for period recovery . . . 29
- 3.7 Performance summary of spectroscopic measurements . . . 30

4 Modelling of Proxima Centauri spectra 33
- 4.1 Plage distribution and results . . . 35
- 4.2 Adding in noise and flares . . . 38

5 Discussion 43

6 Conclusions **47**

A File formats **49**
A.1 Spectral Information File 49
A.2 Equivalent Width Files 49

B Sdadmin program **51**

C Lomb-Scargle Routines **53**
C.1 Numerical Recipes 53
C.2 Scipy, AstroML, Gatspy 54
C.3 Programs and usage 54
C.4 Window functions 55

D TiO Line Measurements **57**

Bibliography **57**

List of Figures

2.1 This is a periodogram calculated from the ASAS database for Proxima Centauri using 970 points of "class A" V-band data from the second aperture. In this periodogram no binning has been applied. The topmost 3 peaks at 82.6 days, 106.4 days and 163.3 are shown and the corresponding FAP values marked in. Periods between 20 and 180 days are considered. 6

2.2 This figure displays the window function of the observation times of the ASAS data from Proxima Centauri as displayed in Fig. 2.1, calculated using *Period04*. There is a strong peak at 0.0027 c/day, which is a period of approximately 370 days. 6

2.3 This figure redisplays together in the upper panel the main peaks in the periodogram of the ASAS data from Proxima Centauri as displayed in Fig. 2.1, calculated using Period04 and on a cycle/day X axis, together with the window function on the same X axis scale in the lower panel. 7

2.4 This is a periodogram calculated from the 624 points remaining (out of the original 970) after the "Class A" V-band data from the ASAS database for Proxima Centauri, using the second aperture, is binned to 1 day. Display is between 20 and 160 days. 8

2.5 This is a periodogram calculated from the 924 points remaining (out of the original 970) after the "Class A" V-band data from the ASAS database for Proxima Centauri, using the second aperture, is binned to 18 minutes. Display is between 20 and 160 days. Note that the Y axis of this is on the same scale as Fig. 2.1 and Fig. 2.4. 8

2.6 This illustrates the phase-folded light curve derived from the 924 points remaining (out of the original 970) after the "Class A" V-band data is binned to 18 minutes and folded to 82.6 days. Some extreme values are omitted in order to show the bulk of the data. A best-fit sinusoidal curve, shown in black, is fitted with baseline 33.12 ± 0.06, phase 0.49 ± 0.02 and amplitude 0.71 ± 0.09. (A scatter plot was considered but the line plot appeared to be easier to follow in this instance, as opposed to Fig. 2.9.) 9

2.7 This is a periodogram derived from the HST data discussed in Benedict et al. (1998) between July 1995 and January 1998 plus some additional points up to January 2001 examining periods showing the three highest peaks and with the FAPs marked in. This has been binned to 4 minutes to eliminate 3 duplicated times. 11

2.8 In the upper panel is displayed a periodogram derived from the same data as Fig. 2.7 calculated with *Period04* and with an X-axis of cycles/day. In the lower panel is displayed the corresponding window function. 11

2.9 Phase-folded light curve, folded to 82.6 days, of HST data discussed in Benedict et al. (1998), with best-fit sine curve fitted, shown in black. This has amplitude 65 ± 7, a phase of 0.45 ± 0.02 and a base level of 4024 ± 5. (A line plot was considered but the scatter plot appeared to be easier to follow in this instance, as opposed to Fig. 2.6). 12

3.1 This figure depicts the Hα region of example spectra of Proxima Centauri taken from HARPS on 27 May 2004 02:10:14 UTC (black) and 15 March 2006 09:16:35 (brown) after normalisation. The region delineated with the dark red solid vertical lines shows the region used for calculation of the Hα equivalent width in this report. The regions shaded in red and blue respectively show the regions used for calculation of the sizes of the two sub-peaks. The solid vertical green lines delineate the region used for calculation of the Hα index in other papers. At the top is displayed the telluric line spectrum for an air mass of 1.4, to which 2.5 has been added for clarity of display. 15

3.2 This figure depicts the earlier of the two example spectra of Proxima Centauri taken from HARPS on 27 May 2004 02:10:14 UTC (black) shown in Fig. 3.1, but selecting a larger region and without normalisation. The solid vertical green lines and green shaded areas in the right panel show the regions for calculation of the Hα index in other papers. The shaded dark green region in the right panel from 6572.468Å to 6573.288Å show the prominent TiO I transition line referred to in Appendix D. 15

3.3 Histogram of equivalent widths for UVES in blue and HARPS in green with the same X axis scale. All the UVES spectra results are shown apart from those for one which appeared to be just noise (12 March 2009 UTC 02:31:11). HARPS spectra are omitted for seven outlying cases which appeared to be dominated by flares. These are listed in Table 3.3. 18

3.4 This figure shows the residuals of the same two spectra as previously shown in Fig. 3.1 after division by the mean of the first five spectra with minimum equivalent width timed at 16 March 2006 UTC 06:37:59, 14 March 2007 UTC 07:28:29, 5 April 2011 UTC 03:26:33, 8 April 2011 UTC 06:28:17 and 22 April 2011 UTC 05:07:46. 19

3.5 Histogram of the residual equivalent widths generated as for Table 3.2 and Fig. 3.4. 19

3.6 This plot is derived from the data from UVES on 10 March 2009. The equivalent width (top panel), peak ratio (second panel) and X-ray data (third and bottom panels) of the Hα flux as shown in Fuhrmeister et al. (2011, Fig. 1). The top two panels are on the same scale throughout. The X-rays displayed are-displayed to the same scale on the fourth panel as for Fig. 3.7 and Fig. 3.8 20

3.7 This plot is derived from the data from UVES on 12 March 2009. The equivalent width (top panel), peak ratio (second panel) and X-ray data (third and bottom panels) of the Hα flux as shown in Fuhrmeister et al. (2011, Fig. 1). The top two panels are on the same scale throughout. The X-rays displayed are-displayed to the same scale on the fourth panel as for Fig. 3.6 and Fig. 3.8 21

3.8 This plot is derived from the data from UVES on 14 March 2009. The equivalent width (top panel), peak ratio (second panel) and X-ray data (third and bottom panels) of the Hα flux as shown in Fuhrmeister et al. (2011, Fig. 1). The top two panels are on the same scale throughout. The X-rays displayed are-displayed to the same scale on the fourth panel as for Fig. 3.6 and Fig. 3.7 22

3.9 This plots show the Hα equivalent width in black and the He-6678 equivalent widths in blue for the HARPS observations during 2013. Vertical scales for Hα and for He-6678 are the same as in Fig. 3.10 and Fig. 3.11. 23
3.10 This plots show the Hα equivalent width in black and the He-6678 equivalent widths in blue for the HARPS observations during 2014. Vertical scales for Hα and for He-6678 are the same as in Fig. 3.9 and Fig. 3.11. 24
3.11 This plots show the Hα equivalent width in black and the He-6678 equivalent widths in blue for the HARPS observations during 2015. Vertical scales for Hα and for He-6678 are the same as in Fig. 3.9 and Fig. 3.10. 25
3.12 This figure shows sample periodograms from the Hα peak of the HARPS data, calculating from equivalent widths using ASTROML for the upper panel and GATSPY for the lower panel. The strongest 5 peaks are highlighted in both cases. 26
3.13 This figure shows a sample periodogram from the peak ratio measure from the Full Set of the data from HARPS binned to 1 day, processed by the GATSPY routine and displayed with the five highest peaks highlighted and showing the values. 27
3.14 In the upper panel is shown the periodogram, displayed in cycles/day, of the equivalent widths from the Original Set of the HARPS data, calculated using *Period04*. In the lower panel is shown the corresponding window function. . . . 28
3.15 In the upper panel is shown the periodogram, displayed in cycles/day, of the equivalent widths from the Full Set of the HARPS data, calculated using *Period04*. In the lower panel is shown the corresponding window function. 28
3.16 In this figure is illustrated the effects of randomly selecting a given proportion of the ASAS data in terms of whether the same period of 82.6 days is recovered and the error in this result. The black vertical dotted lines mark in the proportions of data corresponding to the number of observations remaining in the HARPS data after various clippings and binnings have been performed. 30
3.17 This figure illustrates the relative performance of each of the 4 spectroscopic methods with the Full Set of HARPS data against the "worst" instance of the restriction of the ASAS points as shown in Fig. 3.16. In all cases it is regarded as "success" to recover an 82.6 day period to within 0.5% as one of the largest five peaks of the corresponding periodogram. For each of the four spectroscopic methods considered, all variants of clipping, binning, taking residuals and appropriate combinations of those are collated, to give an overall performance for each measurement method as a percentage. Shown in blue on the spectroscopic results is the percentage to which 82.6 days is recovered. In some cases it was noticed that the 41.3-day sub-harmonic could be recovered and the additional yellow bars denote that proportion of the results in which this was noted (where 82.6 days was not also recovered). 31
3.18 This figure is Fig. 3.17 reworked to illustrate the relative performance of the spectroscopic measurements if periods are regarded as valid to within 2% rather than 0.5% of 82.6 days (or 41.3 days). 32

4.1 Example generated model spectrum of Proxima Centauri, also illustrating the methods for computing the periodicity of spectra. The centre of the Hα line is set at 6563Å for convenience rather than 6562.8Å. The green lines (from 6561.75Å to 6564.25Å) show the limits used for calculation of the equivalent width. The blue and red shaded areas (6561.95Å to 6562.75Å and 6563.44Å to 6564.24Å respectively, each 0.8Å wide) show the regions for calculation of the peak ratio. 34

4.2 This displays simulated spectra showing the extremes and the median value of equivalent width (1.5, 3.0 and 2.3 respectively) with a period of 80 days and an inclination of 80°. The epochs from the HARPS data are used in the model and the selected generated spectra superimposed. 36
4.3 This shows the visible face of the star as generated by DoTS corresponding to the spectra displayed in Fig. 4.2 in chronological order. Left to right, these give the spectra with the median, the lowest and the greatest equivalent widths. . . . 36
4.4 This figure shows the percentage of the correctly recovered period of 80 days as the strongest peak with various levels of SNR and adding various levels of simulated flare data, the blue plot for no flare data. the green plot with the four largest flare data (up to the January 2014) and the red plot the flare data clipped in Section 3.5 as having equivalent width greater than 1 standard deviation from the median in the original data to January 2014. The topmost panel shows the results for an inclination of 30°, the middle panel that for 60° and the bottom panel for 90°. 40
4.5 This figure is effectively the same as Fig. 4.4, but from a starting period of 60 rather than 80 days, showing the significant improvement in the recovery rates with the shorter period. 41
4.6 Example of a periodogram from the modelling simulations after adding noise which returns a peak close to 116.6 days.This was from a case where no flare data was added, to a model based on a period of 80 days, an inclination given of 80° and a SNR of 3. Here 116.5 days appears as the third-strongest peak (highlighted in red). This example gives the strongest peak as 103.7 days, marked in black and the correct period as 80.45 days, marked in green. 42

B.1 The display window of the **Sdadmin** range selection option showing a Proxima Centauri spectrum from HARPS in the Hα region and with various ranges marked in. 52
B.2 The dialog window of the **Sdadmin** range selection option showing the facilities for adjusting the ranges and their display. Each element of the dialog has a popup help message as illustrated. 52

D.1 This shows the section of the first spectrum in the HARPS data (at 27 May 2004 UTC 02:10:14) used for calculating Equivalent Widths and also Peak Ratios from the TiO absorption line from 6572.468Å to 6573.288Å. The blue vertical lines at 6572.463Å and 6572.784Å and the red lines at 6572.797Å and 6573.295Å delineate the regions used for calculation of a version of the Peak Ratios. 57

List of Tables

2.1 Summary of three strongest periods taken from Class A values in ASAS dataset for Proxima Centauri from all apertures based upon magnitudes measured between December 2000 and September 2009. Results are shown for the raw data. 1-day binning and 18-minute binning. 10

2.2 Summary of three strongest periods taken from Class B and lower quality values in ASAS datasets for Proxima Centauri based upon magnitudes measured between December 2000 and September 2009 binned to 18 minutes. 10

3.1 Results for calculation of median and standard deviation Hα equivalent widths (EW), Hα Index and peak ratio (PR) for UVES and HARPS. In the UVES table all the spectra are used and the results shown by day and for all, *apart from an observation clearly consisting of noise only timed at 12/03/09 02:31:11 UTC. In the HARPS table the observations are separated where they are 300 or more days apart. In the summary lines "original set" refers to the observations up to 10/01/2014 and the "full set" also includes data from 19/01/2016 to 30/03/2016. 17

3.2 This table re-displays the HARPS spectra as previously shown in Table 3.1 after calculating the residual spectra from dividing by the mean values of the 5 spectra with the lowest equivalent widths. As before, the rows marked † show where equivalent widths of greater than 2 standard deviations from the median are removed and the median and standard deviations recalculated. 18

3.3 This table lists, in descending order of Hα equivalent width, the seven spectra mentioned in Section 3.2 and Fig. 3.3 as having equivalent widths over 6.0 (and not displayed in that figure). As well as showing the values of the Hα equivalent width, that of the He-6678 line is also displayed. This table also shows the seven spectra having the He-6678 line with the largest equivalent width, five of which, not marked with * or †, are common to the set of seven with largest Hα. The two remaining out of the seven with exceptional Hα but not an exceptional He line are marked with * and vice versa for the ones marked with †. 23

4.1 Simulated mean equivalent widths with associated standard deviations from simulations for the 2.7% plage distributions and a set of rotation periods and inclinations. In the first table results are illustrated for various periods and for 30°, 60° and 90° inclinations. In the second table results are illustrated for various inclinations and 70, 80 and 90-day periods as these are close to the rotation period of Proxima Centauri. 37

D.1 Results for calculation of median and standard deviation of the equivalent widths of the TiO transition at 6572.468Å to 6573.288Å from HARPS. The observations are separated where they are 300 or more days apart. 58

List of Abbreviations

ASAS	**A**ll **S**ky **A**utomated **S**urvey
EW	**E**quivalent **W**idth
ESO	**E**uropean **S**outhern **O**bservatory
FAP	**F**alse **A**larm **P**robability
HARPS	**H**igh **A**ccuracy **R**adial velocity **P**lanet **S**earcher
PR	**P**eak **R**atio
SNR	**S**ignal to **N**oise **R**atio
UVES	**U**ltraviolet and **V**isual **E**chelle **S**pectrograph
VALD	**V**ienna **A**tomic **L**ine **D**atabase

Chapter 1

Introduction

1.1 The importance of the study of M-dwarf stars

M-dwarf stars are particularly important as a field of study. One major reason for this is that they account for over 75% of the stars within 25 pc of the Sun, as described in Winters et al. (2015). Indeed our nearest neighbour, Proxima Centauri, is an M5.5V star. Studies such as van Dokkum and Conroy (2010) have argued for a similar proportion of M-dwarf stars in galaxies other than the Milky Way, although that paper concedes the impossibility of observing them individually as, for example, a star such as Barnard's star with an absolute magnitude of about 13 would have a K band magnitude of about 39 at the distance of the Virgo cluster. The stellar populations of other galaxies is a field of considerable interest in itself, but one well outside the scope of this report.

M-dwarf stars are also of great interest in the search for exoplanets. Having lower mass than earlier type stars, the radial velocity variations induced by planetary orbits is proportionally greater. In Johnson et al. (2007), it is seen that the likelihood of planets approaching Earth-size is actually higher than for G or K stars and in Barnes et al. (2012) a search for such planets in the habitable zone of M-dwarfs was undertaken. In both Barnes et al. (2014) and Tuomi et al. (2014) the likelihood of such planets in the habitable zone of M-dwarfs is taken further. The habitable zone of the much cooler M-dwarfs would obviously be much closer to the stars than the Sun, less than 0.1 AU, with complications such as tidal locking of planets and their exposure to flares. Despite these drawbacks to habitability, the longevity of the much slower burning

M-dwarfs by comparison with earlier spectral type stars would increase the opportunities for biological evolution to take hold at some stage.

In the search for the periodic signatures of exoplanets, it is obviously necessary to distinguish between those and the rotation period of the star itself. The orbital period of exoplanets of particular interest, as being potentially in the habitable zone close to an M-dwarf, is of the order of around 10 days, shorter than the 24-day rotation period of the sun. Also, as observed later in this report, aliases can arise from the combination of two or more different periods. This has been the focus of intensive debate in recent papers which have expressed quite divergent views regarding whether reported planets have been validly detected by their period such as in Barnes et al. 2013; Robertson et al. 2014; Robertson and Mahadevan 2014; Tuomi and Anglada-Escudé 2013; Robertson et al. 2015b.

1.2 Activity and the rotation period

Despite their abundance, many aspects of the activity of M-dwarfs have remained less well characterised compared to other classes of star, mainly because of their inherent faintness. Stars become fully convective below around M4V and the transition to this regime has been a subject of some study, as for example the conference proceedings of Stassun et al. (2011).

Of particular interest is the study of complex magnetic activity in such stars and consideration of the dynamo systems which would give rise to this. Authors such as Morin et al. (2011) argue for two simultaneous dynamos, whereas Kitchatinov et al. (2014) discount this and argue for some of the observed activity being due to magnetic field inversions.

In Mohanty and Basri (2003) the authors set out the correlation between the projected rotational velocity $V_{\rm eq} \sin i$ and the activity in mid-M to L-dwarfs, charting activity against rotational velocity up to about 12 km/s where a saturation velocity is observed. They also note an increase in rotation velocities for later stars and a drop-off in activity for L-dwarfs. This is developed further in Reiners and Basri (2008) and also Schmidt et al. (2015), however the latter disagree with the previously-reported drop-off in activity for L-dwarfs, arguing that dust affects the measurements of activity, reporting activity in L-dwarfs down to L6.

In Mohanty et al. (2002) the relation between activity and rotational velocity is explored, however both in this and in Mohanty and Basri (2003) the authors state that the correlation between

rotation and activity is not as strong in fully convective stars from M3 on and suggest that a "turbulent dynamo" is responsible.

It is clear that the measurement of rotational velocity is of importance for a full understanding of these processes.

1.3 The importance of Hα

The Hα line is a powerful diagnostic tool in many areas of astronomy. For example, Hα luminosity is one of the key ways of estimating the star formation rates in galaxies (see for example Rosa-González et al. (2002)). In terms of the study of stars, since the core of Hα forms above the photosphere, as shown in Vernazza et al. (1981), it is an important line for studying activity and variability in stellar chromospheres (Hall, 2008). Chromospheric features such as plage regions and jets are seen well in Hα (see for example Kneer (2010) and Kuridze et al. (2011)). The behaviour of the Hα line in M-dwarf stars is seen as a key diagnostic of activity, as shown in the previously-cited papers (Mohanty et al. 2002; Mohanty and Basri 2003; Reiners and Basri 2008; Schmidt et al. 2015) which describe the relationship between rotation and activity.

The behaviour of the Hα line is a potentially important diagnostic because it is sensitive to magnetic activity and is a strong line usually seen in emission in later M-dwarf stars. It is used as the measure of activity in, for example Mohanty and Basri (2003) and subsequent papers. In Hatzes (2016) the Hα periodicity is explicitly studied in relation to GL 581 and whether the exoplanet GL 581d is indeed real or is actually an alias, which has been debated extensively – see Barnes et al. 2013; Robertson et al. 2014; Tuomi and Anglada-Escudé 2013; Robertson et al. 2015a.

This report investigates whether periodicity can be identified in the morphology of the Hα line obtainable from high-resolution spectra such as those obtained from the *Ultraviolet and Visual Echelle Spectrograph* (UVES) at the 8.2m Very Large Telescope (VLT, UT 2) and the *High Accuracy Radial velocity Planet Searcher* (HARPS) at the ESO La Silla 3.6m telescope. Barnes et al. (2014) noticed that while a strong transient emission in Hα was observable during flares, it should nevertheless be possible to derive periodicity from the morphology of the Hα line. On the other hand, it must be said that in Reiners (2009), the authors suggest that Ca, He and Hα lines, being chromospheric emissions, are strongly affected by activity and should be omitted when searching for radial velocities in active M-dwarfs.

Conscious of these divergent views, this report attempts to study the merits of precision measurements using chromospheric features and in particular Hα analysis.

1.4 Proxima Centauri

As the nearest star to the solar system at a distance of 1.3 parsecs, Proxima Centauri is a bright M5.5V star with a magnitude of 11.13 in the V-band and is of obvious interest with extensive data sets available. The Hα line is always in emission with a characteristic shape. Thus is it a good place to test the general methodology applicable to late M-dwarfs.

Proxima Centauri is part of a system of three stars together with Alpha Centauri A and B and of higher metallicity than the Sun, as described in Linsky et al. (2004). This further focuses interest on the search for rocky planets and ones to be found in the habitable zones of those stars, with one recently discovered for Proxima Centauri and reported in Anglada-Escudé et al. (2016).

Despite the interest and available data, the rotation period of Proxima Centauri is nevertheless uncertain. Previous studies have reported periods ranging from the 31.5 ± 1.5 days of Guinan and Morgan (1996), the 41.3 days of Benedict et al. (1993) and s between 82 and 84 days in Benedict et al. 1992, 1998. Kürster et al. (1999) found that the period is not less than 50 days, whilst more recently Kiraga and Stepien (2007) reported a value of 82.5 days. All these estimates were based on photometric measurements. In Cincunegui et al. (2007) a 447-day activity cycle is reported, based upon Hα measurements. Latterly Suárez Mascareño et al. (2015, Table 3) reported a value of 116.6 days, again using a measurement of Hα.

Proxima Centauri has quite frequent flares and whilst they obviously disturb the measurements, they enable a study to be made of and to what extent they compromise methods for the calculation of the rotation period.

1.5 Methodology

The approach taken in this report is as follows is similar to that taken by Giguere et al. (2016) for the K dwarf ε Eridani. In Chapter 2 photometric measurements of the periodicity of Proxima Centauri are examined, as these prove a useful benchmark for spectroscopic measurements. In Chapter 3 the measurement methods are introduced which are subsequently used to investigate

periodicity from sets of spectra. In Chapter 4 possible models of Proxima Centauri are studied and attempts are made to apply the measurement methods to simulated spectra to evaluate their performance, obtain error estimates and determine how these vary with poorer signal to noise ratio. Chapter 5 and 6 report the discussion and conclusions of this study. Appendices describe some of the software tools developed and used and list some additional results.

Chapter 2

Periodicity from photometric measurements

To process the data for all the periodicity studies in this report, all but one item[1] of the associated software was written in Python using the Lomb-Scargle routines described in Appendix C.

As nearly all previous measurements of periodicity in Proxima Centauri were made using photometric observations, in this report, before discussing spectroscopic measurements such as with the HARPS data and the various methods of analysing the Hα lines, some photometric observations for Proxima Centauri are considered.

2.1 ASAS

First are presented results obtained from the photometric observations of Proxima Centauri taken in the V-Band (there were no data for the I-Band) from the All Sky Automated Survey (ASAS), (Pojmanski, 1997), which comprises data obtained between the dates December 2000 to September 2009.

The data acquired by ASAS is collected via five apertures from 2 to 6 pixels wide. The ASAS guidelines[2], recommend the selection of an aperture appropriate to the magnitude of the target object in the selected band and suggest a formula for doing so. Following these guidelines, taking into account that Proxima Centauri has magnitude 11 in the V-band, the dataset from the

[1] The *Numerical Recipes* Lomb-Scargle program, the Fortran version of which was modified and used.
[2] These are described in http://www.astrouw.edu.pl/asas/explanations.html

second (3 pixel) aperture was selected. Fig. 2.1 shows the Lomb-Scargle periodogram obtained from the 970 measurements of the "best" (grade A) data from this aperture, using the *Numerical Recipes* routine, which returns false alarm probabilities (FAP). The range of periods from 20 to 180 days is considered, to take into account the possibility that the 82.6-day period might be a sub-harmonic of the true period.

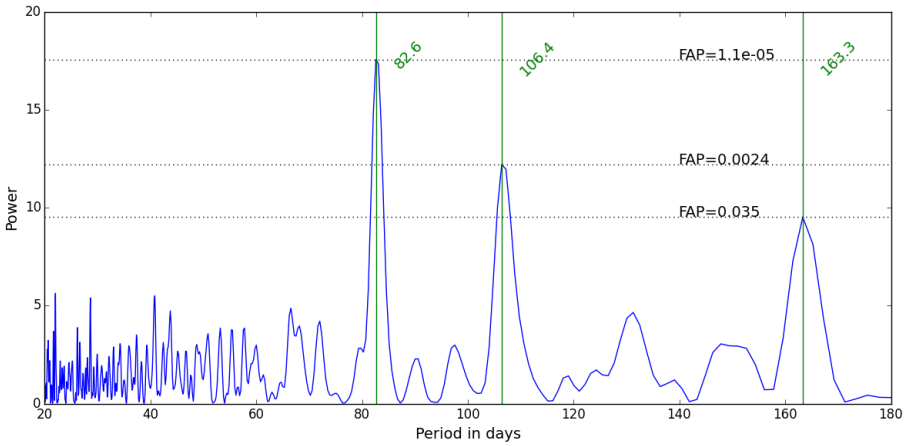

FIGURE 2.1: This is a periodogram calculated from the ASAS database for Proxima Centauri using 970 points of "class A" V-band data from the second aperture. In this periodogram no binning has been applied. The topmost 3 peaks at 82.6 days, 106.4 days and 163.3 are shown and the corresponding FAP values marked in. Periods between 20 and 180 days are considered.

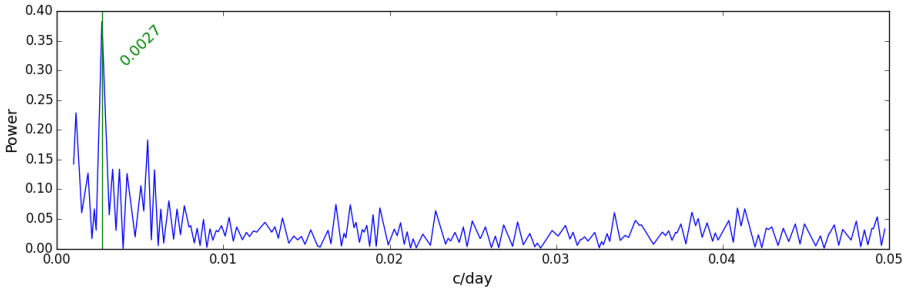

FIGURE 2.2: This figure displays the window function of the observation times of the ASAS data from Proxima Centauri as displayed in Fig. 2.1, calculated using *Period04*. There is a strong peak at 0.0027 c/day, which is a period of approximately 370 days.

The 163.3-day period is close to double the 82.6-day period reported in the papers previously discussed and given here as the strongest peak and has a poorer FAP. It was therefore considered that the 82.6-day period was not likely to be a sub-harmonic of this.

In Fig. 2.2 is displayed the window function of the observation times of this data, calculated using *Period04*[3], showing a clear peak of 0.0027 c/day, equivalent to a period of 370 days[4]. It

[3]Obtainable from https://www.univie.ac.at/tops/Period04/

[4]The periods given by *Period04* are up to 1.3% different from the Lomb-Scargle based routines.

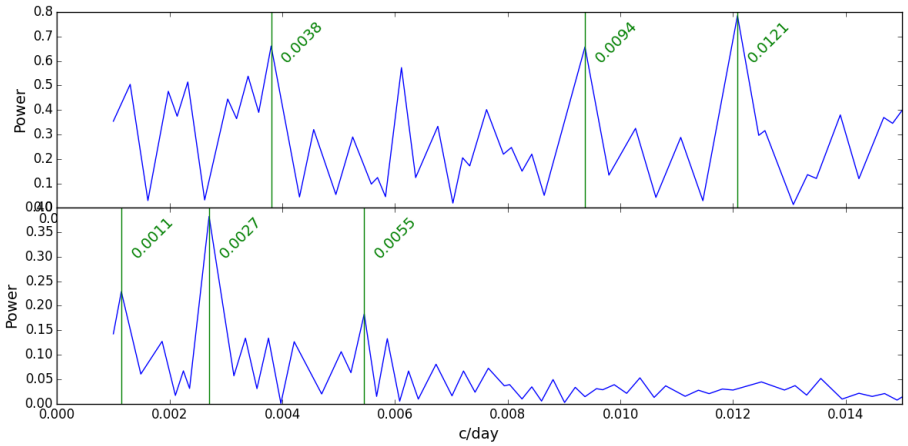

FIGURE 2.3: This figure redisplays together in the upper panel the main peaks in the periodogram of the ASAS data from Proxima Centauri as displayed in Fig. 2.1, calculated using Period04 and on a cycle/day X axis, together with the window function on the same X axis scale in the lower panel.

was also found useful to re-plot the periodogram and the window function on the same scale, as shown in Fig. 2.3, calculated using *Period04*, as the window function shows the same clear peak of 0.0027. Subtracting this frequency from the strongest period of 0.0121 c/day in the periodogram (corresponding to the 82.6-day period) gives 0.0094 c/day, which is the next strongest peak in the periodogram corresponding to the 106.3-day period in Fig. 2.1. Taking into account the methods described in Dawson and Fabrycky (2010), it is possible to express confidence that 82.6 days is a genuine period and the 106.3 day period an alias in consequence of the strong 0.0027 c/day peak in the window function.

As some of the observations were duplicated or apparently overlapping, these were initially binned to 1 day, in line with several of the HARPS results described in Section 3.5. This reduced the number of points to 624. From the result the periodogram shown in Fig. 2.4 was obtained. This appeared to clarify the peaks by reducing the number with very short periods and enhancing the two major ones. Some binning appeared to be necessary as some of the points had duplicated times. It appeared worthwhile to experiment with sizes of binning to see at what point the result was optimal, in terms of yielding the strongest peaks with the lowest FAP and least extraneous peaks and after trying various binning values between several days down to 1 minute, the optimal binning was found to be 18 minutes, yielding the periodogram shown in Fig. 2.5. Note that the scale of this is the same but the figure has been made taller to accommodate the more powerful 82.6 day peak. The reduction of the points in the binning to 18 minutes was found to be a much more modest reduction, to 924 observations from 970. The explanation of this 18-minute

binning result may be related to the 3-minute exposure time for ASAS 3 (Pojmański, 2001).

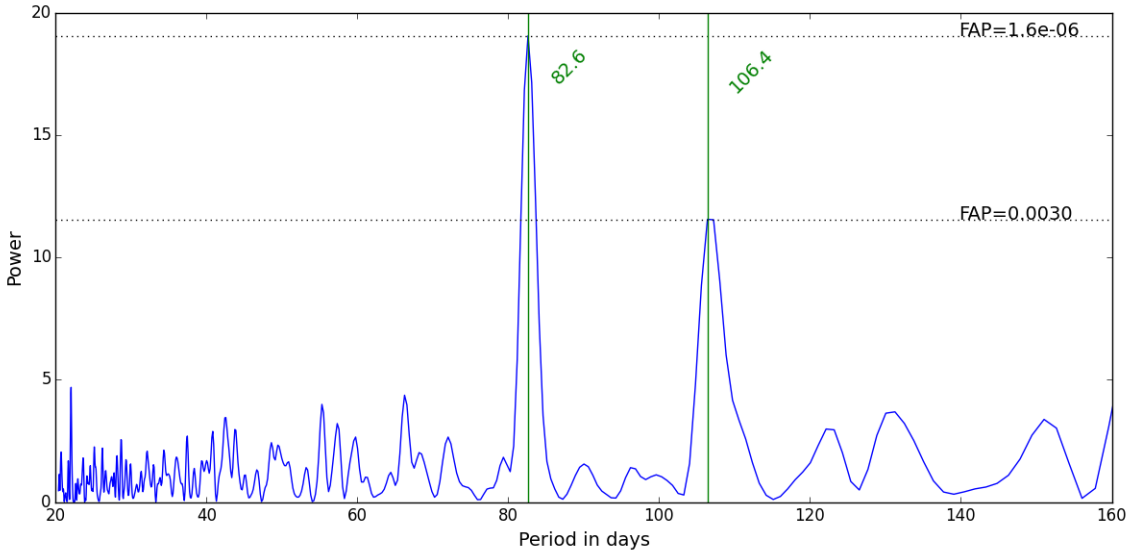

FIGURE 2.4: This is a periodogram calculated from the 624 points remaining (out of the original 970) after the "Class A" V-band data from the ASAS database for Proxima Centauri, using the second aperture, is binned to 1 day. Display is between 20 and 160 days.

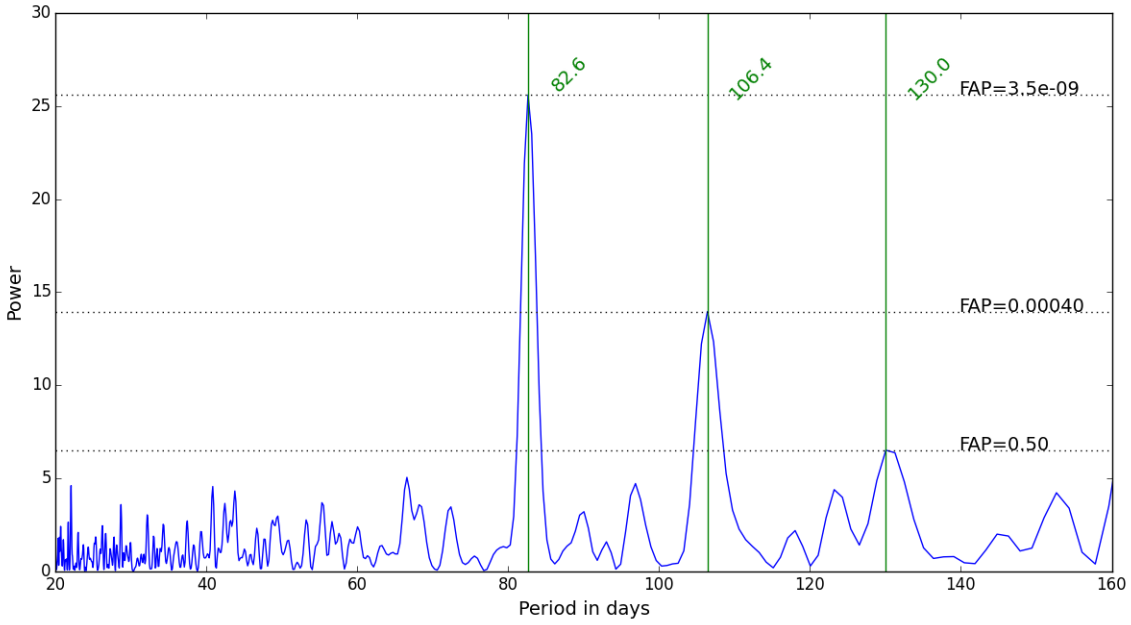

FIGURE 2.5: This is a periodogram calculated from the 924 points remaining (out of the original 970) after the "Class A" V-band data from the ASAS database for Proxima Centauri, using the second aperture, is binned to 18 minutes. Display is between 20 and 160 days. Note that the Y axis of this is on the same scale as Fig. 2.1 and Fig. 2.4.

Construction of a phase-folded light curve from the 18-minute binned data yields Fig. 2.6.

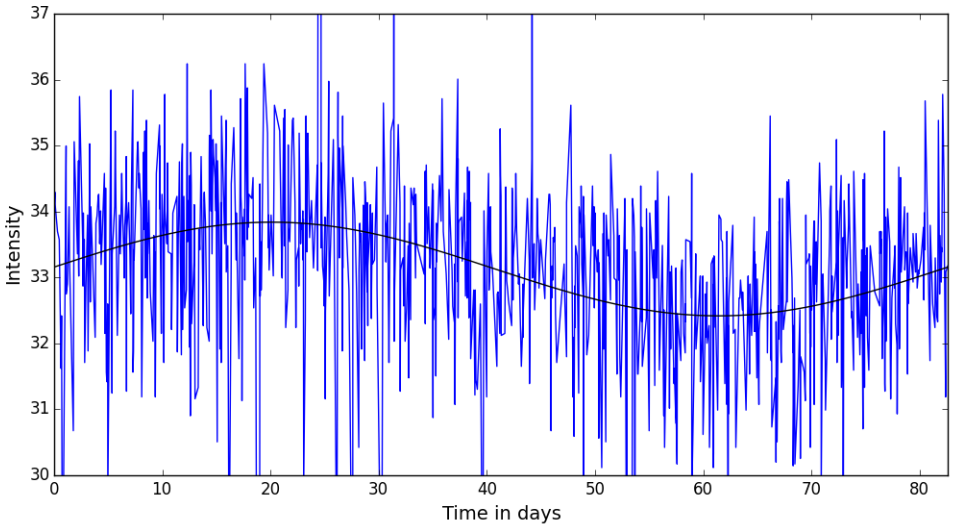

FIGURE 2.6: This illustrates the phase-folded light curve derived from the 924 points remaining (out of the original 970) after the "Class A" V-band data is binned to 18 minutes and folded to 82.6 days. Some extreme values are omitted in order to show the bulk of the data. A best-fit sinusoidal curve, shown in black, is fitted with baseline 33.12 ± 0.06, phase 0.49 ± 0.02 and amplitude 0.71 ± 0.09. (A scatter plot was considered but the line plot appeared to be easier to follow in this instance, as opposed to Fig. 2.9.)

Although the recommended aperture by ASAS for Proxima Centauri is the second aperture, it appeared valuable to compare the three highest peaks from each of the apertures finding that nearly all the data gave a first peak of 82.6 days, a second peak of 106.4 days and a much less significant third peak (over 0.5 FAP) of about 131 days in most cases. The results are listed with no-binning, 1-day and 18-minute binnings in Table 2.1. Also considered were the other grades of ASAS data[5], with a little under half of the Class A data, 416 points and much higher error rating. All the periodograms from this lower quality data still showed a strong peak of around 83 days. The results (for 18-minute binning only) are shown in Table 2.2.

It was noticeable that all of the Lomb-Scargle routines listed in Appendix C gave exactly the same results (apart from differences to scaling of the power) with all the ASAS data, including the lower quality data. This was in contrast to the spectroscopic results discussed in later chapters of this report.

A search was made for very long periods up to the period spanned by the data in each case, however no strong periods could be found, in particular nothing close to the 442 days reported in Cincunegui et al. (2007)[6].

[5]These are mostly from ID 142944-6241.0.

[6]No such period was found in the HST or spectroscopic results either.

Aperture	binning	Peak 1 (days)	Peak 2 (days)	Peak 3 (days)
1	none	83.1	106.4	131.3
2	none	82.6	106.4	22.0
3	none	82.6	106.4	131.3
4	none	82.6	106.4	131.3
5	none	82.6	106.4	131.3
1	1 day	82.6	106.4	110.6
2	1 day	82.6	106.4	22.0
3	1 day	82.6	106.4	130.0
4	1 day	82.6	106.4	42.6
5	1 day	82.6	106.4	42.4
1	18 min	83.1	106.4	131.3
2	18 min	82.6	106.4	130.0
3	18 min	82.6	106.4	130.0
4	18 min	82.6	106.4	130.0
5	18 min	82.6	106.4	131.3

TABLE 2.1: Summary of three strongest periods taken from Class A values in ASAS dataset for Proxima Centauri from all apertures based upon magnitudes measured between December 2000 and September 2009. Results are shown for the raw data. 1-day binning and 18-minute binning.

Aperture	Peak 1 (days)	FAP	Peak 2 (days)	FAP	Peak 3 (days)	FAP
1	83.1	0.0067	105.8	0.33	127.4	0.82
2	83.1	0.03	105.8	0.43	127.4	0.61
3	83.1	0.038	105.8	0.31	128.7	0.89
4	84.1	0.1	105.8	0.21	128.7	0.93
5	84.1	0.0024	105.8	0.0028	82.5	0.0033

TABLE 2.2: Summary of three strongest periods taken from Class B and lower quality values in ASAS datasets for Proxima Centauri based upon magnitudes measured between December 2000 and September 2009 binned to 18 minutes.

2.2 HST

As another source of photometric results, periodograms were derived from the HST data discussed in Benedict et al. (1992) and in Benedict et al. (1998) consisting of 171 points obtained between July 1995 and January 1998, later enhanced so the last 18 points extended to January 2001. The data used a filter centred on 583nm with 234nm FWHM (Benedict et al., 1998). Three times were actually duplicated and eliminating the duplications (taking the mean value), it was possible to obtain the periodogram in Fig. 2.7.

Again, as with the ASAS data, all the Lomb-Scargle routines listed in Appendix C gave almost identical periodograms (other than the scaling of the power). A phase-folded light curve of this is displayed in Fig. 2.9. Calculation of the window function of these observation times gave the result shown in Fig. 2.8.. The window function peak at 0.0007 cycles/day would appear to account for the peak of around 78 days in Fig. 2.7 which corresponds to 0.0129 cycles/day in the in upper panel of Fig. 2.8.

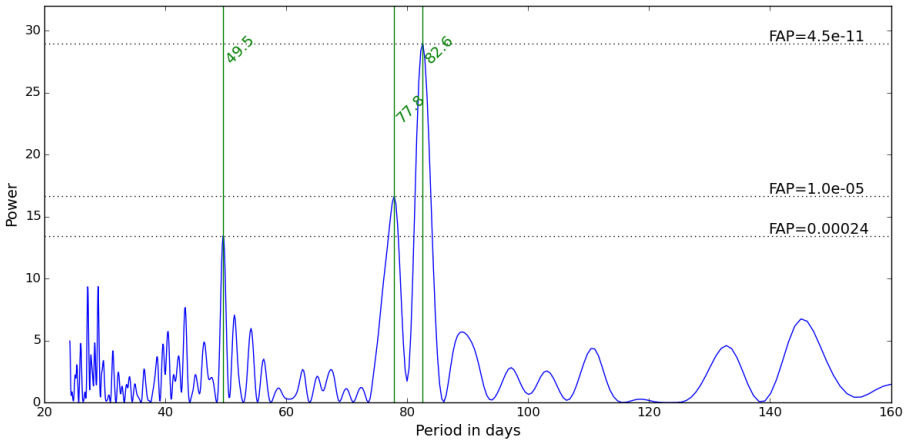

FIGURE 2.7: This is a periodogram derived from the HST data discussed in Benedict et al. (1998) between July 1995 and January 1998 plus some additional points up to January 2001 examining periods showing the three highest peaks and with the FAPs marked in. This has been binned to 4 minutes to eliminate 3 duplicated times.

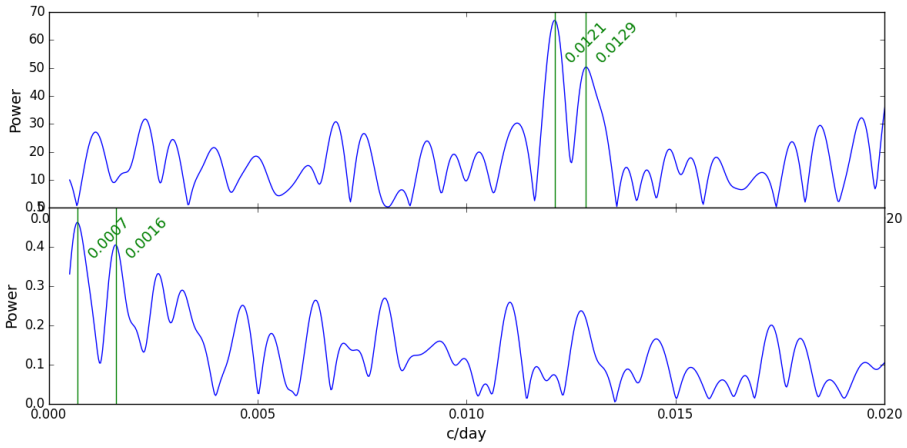

FIGURE 2.8: In the upper panel is displayed a periodogram derived from the same data as Fig. 2.7 calculated with *Period04* and with an X-axis of cycles/day. In the lower panel is displayed the corresponding window function.

2.3 Summary of photometric results

The period at 82.6 days is clearly as a strong, very low-FAP peak in both the ASAS and HST data. It is almost certainly the rotation period of Proxima Centauri, seemingly with a small error bar, although some investigations in Section 3.6 were undertaken partly to investigate this.

It also provides a convenient benchmark for assessing the accuracy and reliability of the other, less clear spectroscopic methods investigated in Chapter 3 based on the Hα line.

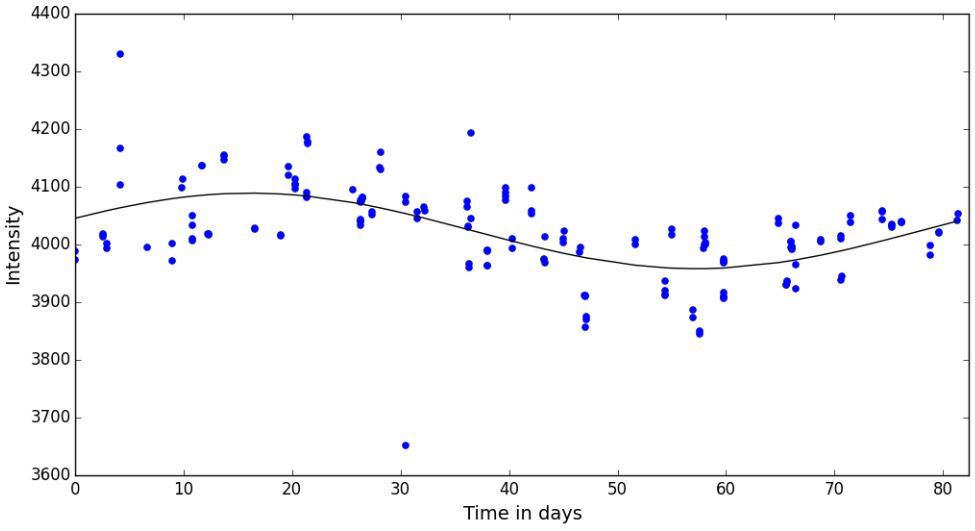

FIGURE 2.9: Phase-folded light curve, folded to 82.6 days, of HST data discussed in Benedict et al. (1998), with best-fit sine curve fitted, shown in black. This has amplitude 65 ± 7, a phase of 0.45 ± 0.02 and a base level of 4024 ± 5. (A line plot was considered but the scatter plot appeared to be easier to follow in this instance, as opposed to Fig. 2.6).

The ASAS data, including the lesser quality data also included a strong peak at 106.4 days but this was not seen on the HST data. The former, however, has observation times much more constrained by the time of year and it is noticeable that:

$$\frac{1}{\frac{1}{82.6} - \frac{1}{365.25}} = 106.7$$

This corresponds to the findings from the study of the window function in Fig. 2.3. Similarly the strong 77.8-day period seen in the HST data but not in the ASAS data appears to be related to the 0.0007 cycles/day peak in the window function illustrated in Fig. 2.8, so again it is concluded to be an alias thrown up by the observation times.

Chapter 3

Spectra of Proxima Centauri

Two sources of spectra for Proxima Centauri are considered in this report, those from UVES taken between 10 and 14 March 2009 studied in Fuhrmeister et al. (2011) and HARPS spectra with 260 data points between May 2004 and January 2014 from the ESO archive[1] and referenced in Suárez Mascareño et al. (2015, Table 3). The latter were supplemented with 56 additional spectra from HARPS taken between 19 January and 30 March 2016[2]. The UVES data were obtained with a 0.8 or 1.10" slit, yielding a resolving power of approximately 60,000., while the resolution of HARPS is approximately 120,000. Also studied in Section 3.3 are the X-ray data from XMM-Newton used in the Fuhrmeister et al. (2011) paper[3] to identify any association between strong X-ray emission and possible corresponding changes to the Hα profile.

The bulk of the results from HARPS in this chapter are taken using the full set of data up to 30 March 2016. However reference is made to the original set to January 2014 ("Original Set") as this is necessary to reproduce previous calculations of the rotation period of Proxima Centauri, in particular the 116.6 days reported by Suárez Mascareño et al. (2015, Table 3), which is not reproducible from the full set to March 2016 ("Full Set"). The observation times in the Original Set are used in the modelling results in Chapter 4 as nearly all the work on the modelling was completed prior to 2016.

[1] Based on data obtained from the ESO Science Archive Facility from programs 072.C-0488(E), 082.C-0718(B), 183.C-0437(A) and 191.C-0505(A).

[2] Based on data obtained from the ESO Science Archive Facility from programs 096.C-0082(A) through to 096.C-0082(F).

[3] Provided by Fuhrmeister, priv. comm.

3.1 HARPS and UVES spectra of Proxima Centauri

As mentioned in Mohanty and Basri (2003) and subsequent papers such as Jenkins et al. (2009) and Barnes et al. (2014), the spectra of late M-dwarfs from approximately M5 onward, usually show Hα in emission. Several of the M-dwarfs illustrated in Barnes et al. (2014, Fig. 6) additionally show a distinct "horned" appearance, due to self-absorption at the centre of the Hα peak. Proxima Centauri consistently shows this pattern, which is displayed in Fuhrmeister et al. (2011, Fig. 14). The two sub-peaks surround a local minimum. Not only does the equivalent width of the entire Hα peak, vary in time, but the two sub-peaks also vary in relative size over time. The local minimum between the sub-peaks, however, does not appear to vary greatly over time. This would appear to be because a more symmetrically-distributed spectral line from the photosphere is overlaid with plage and chromospheric effects which are asymmetric or localised to regions. These may be compared with the H, K and Ca II lines discussed in Rauscher and Marcy (2006). The main aim of this report is to study the variations in the line and sub-peaks via various methods to see if periodicity may be reliably recovered.

3.2 Hα line measurements

In Fig. 3.1 are shown two example spectra from HARPS nearly 2 years apart, clearly showing the changes in the amplitude and shape of the Hα line. Fig. 3.1 also illustrates the regions used to investigate periodic variability.

The spectra were first normalised by iteratively fitting a cubic polynomial to all the points in all the spectra, apart from the Hα region, then excluding points outside 2 standard deviations above or below the fitted polynomial to eliminate other lines, both emission and absorption. The computations discussed in this report are then calculated from these normalised spectra.

Fig. 3.1 illustrates the regions used to calculate various measurements discussed in this report. To calculate equivalent widths of the Hα peak, points in the range delineated by the dark red solid lines are considered, running from 6561.917Å to 6563.839Å, linearly interpolating points in each spectrum up to the boundaries of the region to minimise integer pixel noise effects. The area of this region is then calculated using trapezoidal integration and the value of the equivalent

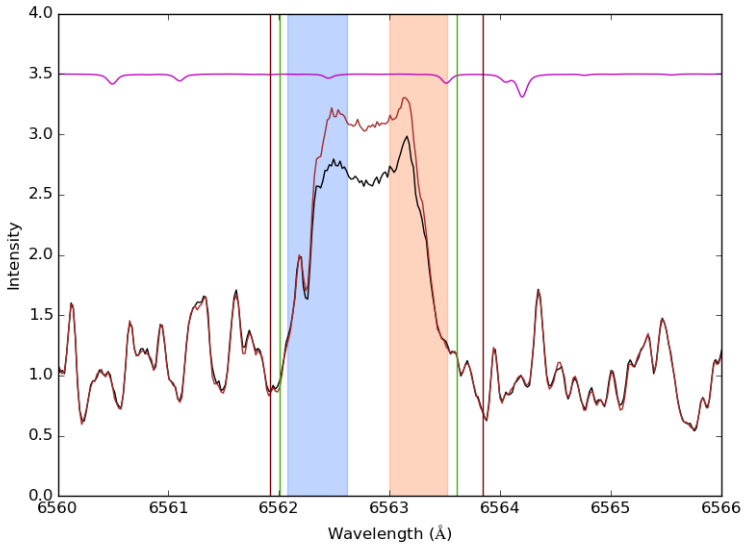

FIGURE 3.1: This figure depicts the Hα region of example spectra of Proxima Centauri taken from HARPS on 27 May 2004 02:10:14 UTC (black) and 15 March 2006 09:16:35 (brown) after normalisation. The region delineated with the dark red solid vertical lines shows the region used for calculation of the Hα equivalent width in this report. The regions shaded in red and blue respectively show the regions used for calculation of the sizes of the two sub-peaks. The solid vertical green lines delineate the region used for calculation of the Hα index in other papers. At the top is displayed the telluric line spectrum for an air mass of 1.4, to which 2.5 has been added for clarity of display.

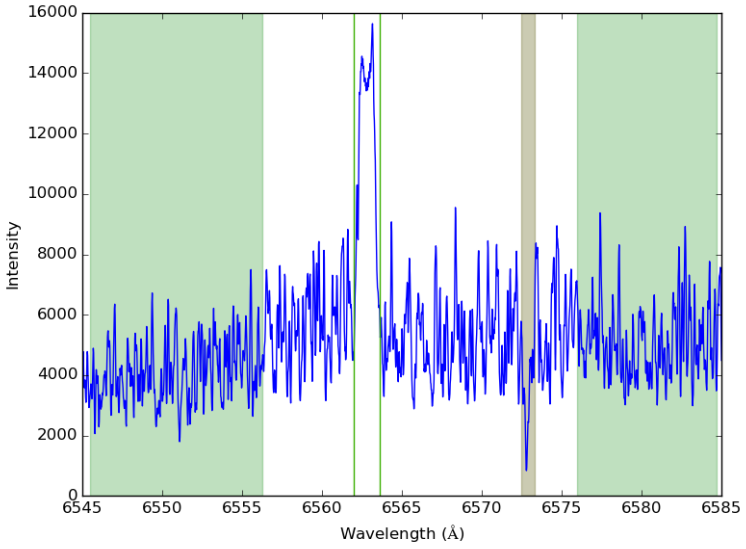

FIGURE 3.2: This figure depicts the earlier of the two example spectra of Proxima Centauri taken from HARPS on 27 May 2004 02:10:14 UTC (black) shown in Fig. 3.1, but selecting a larger region and without normalisation. The solid vertical green lines and green shaded areas in the right panel show the regions for calculation of the Hα index in other papers. The shaded dark green region in the right panel from 6572.468Å to 6573.288Å show the prominent TiO I transition line referred to in Appendix D.

width is calculated as the width (in Å) of the rectangle of the same area whose height would be 2, i.e., 1 above the normalised continuum[4].

Also calculated is what is herein called the "Peak Ratio", defined as the ratio of the mean values of the two sub-peaks. The ratio tabulated below is the mean value of the flux at each point in "red" sub-peak,, divided by the mean value of the flux at each value in "blue" sub-peak. The regions selected for the blue and red sub-peaks are shaded in blue and red in Fig. 3.1 and run from 6562.072Å to 6562.613Å and 6563.000Å to 6563.517Å respectively. These do not have to be the same widths, the "blue" sub-peak region having a width of 0.541Å and the "red" sub-peak region a width of 0.517Å. This is because the peak ratio measurement utilises the mean values of the selected points, which proved not to be very sensitive to the actual number in the selected range, hence the regions were chosen to optimise variability in the line profiles as in the observed data the "red" sub-peak tends to be higher but narrower than the "blue" sub-peak. For similar reasons, there is no need to interpolate points to the boundaries of the region for the peak ratio measurement.

The number of pixels in the regions, as highlighted in Fig. 3.1 are either 35 or 36 for the Hα region and 11 or 12 for the red sub-peak and 14 or 15 for the blue sub-peak on UVES. The corresponding numbers on HARPS are 98 or 99, 26 or 27 and 27 or 28 respectively. The number of pixels could vary by one due to differing wavelength corrections caused by the barycentric component of the radial velocities.

In Fig. 3.1, at the top, is displayed the telluric line spectrum for an air mass of 1.4, to which 2.5 has been added for clarity of display. As demonstrated in Reiners et al. (2015, Fig. 1), the telluric effects are negligible in this region. (The Gaussian used to simulate Hα in that paper is considerably broader than that observed in Proxima Centauri, so the telluric line at 6564.2Å can impinge on the former but not Proxima Centauri.) All the spectral lines identifiable from the Vienna Atomic Line Database (VALD) are TiO transitions, with the exception of a MgH line at 6564.29Å.

In Suárez Mascareño et al. (2015), the authors use an *Hα index*, based in turn upon the work in Gomes da Silva et al. (2011), computed by the formula:

$$H\alpha_{index} = \frac{H\alpha_{core}}{H\alpha_L + H\alpha_R}$$

[4]It is accepted the equivalent widths are normally negative for emission lines, but in this report this calculation is used to return analogous positive values throughout.

In this $H\alpha_{core}$ is defined as the flux in the bandpass of width 1.6Å centred on 6562.808Å and $H\alpha_L$ and $H\alpha_R$ are defined respectively as continuum bands of widths 10.75Å and 8.75Å centred on 6550.87Å and 6580.31Å. That $H\alpha_{core}$ region is delineated by the solid green vertical lines in both Fig. 3.1 and Fig. 3.2 and the two continuum regions as the green shaded areas in Fig. 3.2. An important difference between this and calculation of the equivalent widths and peak ratios is that the spectra do not have to be normalised for the Hα Index calculation as the calculation supplies its own normalisation.

The region chosen for calculation of the Hα equivalent width in this report is slightly wider than that chosen for the Hα index in the Suárez Mascareño et al. (2015). This was chosen as it appeared on-average to encompass the whole of the Hα peak more accurately and to better record the variations. In practice, there was negligible difference between the calculated results for either method using the two pairs of limits. Adjusting the continuum ranges used for calculation of the Hα Index to cover much wider ranges, including the entire area of that spectral order clear of the Hα peak, whilst yielding different values, the proportionate ranges were very similar and it made negligible difference (less than 0.1%) to the periodicity calculations.

In Table 3.1 are listed the equivalent widths, Hα Index and peak ratios from the UVES and HARPS data for Proxima Centauri. Histograms of the equivalent widths are shown in Fig. 3.3. Note that all the equivalent widths from the UVES data are displayed, but the seven very highest from the HARPS data are omitted, which have equivalent widths of over 6, which are listed in Table 3.3. These were omitted from Fig. 3.3 as their display would have caused Fig. 3.3 to be too wide for no particular benefit.

Bearing in mind the study of kurtosis in Hα in Flores et al. (2016) for HD 45184, for this report other possible calculations of periodicity were derived from skewness and kurtosis of the Hα peak and from residual Hα lines. The residuals were created by division of each spectrum by mean of the 5 spectra with the lowest equivalent widths. In Table 3.2 are recalculated the figures for the median residual equivalent widths and peak ratios for HARPS which were previously displayed in Table 3.1. The same two spectra which are displayed in Fig. 3.1 are re-displayed after this treatment in Fig. 3.4. A histogram of the residual equivalent widths is displayed in Fig. 3.5.

The spectra from HARPS also contained a prominent absorption line in the same spectral order as the Hα line. This can be seen shaded in dark green in Fig. 3.2. Identifying this from VALD as primarily a TiO transition, it seemed worth looking briefly to see if the equivalent width

Spectra	From	To	No.	EW	Hα Ind	PR
UVES	10/03/2009	(same)	215	1.759 ± 0.301	1.759 ± 0.301	0.850 ± 0.021
	12/03/2009	(same)	*166	1.324 ± 0.258	1.324 ± 0.258	0.907 ± 0.014
	14/03/2009	(same)	179	1.492 ± 0.560	1.492 ± 0.560	0.921 ± 0.025
	ALL		560	1.570 ± 0.428	1.570 ± 0.428	0.899 ± 0.036
HARPS	27/05/2004	21/07/2004	6	2.711 ± 7.105	0.248 ± 0.416	1.013 ± 0.024
	25/07/2005	22/03/2006	5	1.407 ± 0.479	0.176 ± 0.027	0.975 ± 0.011
	14/03/2007	19/07/2007	5	2.012 ± 0.542	0.210 ± 0.031	0.999 ± 0.010
	29/06/2008	06/04/2010	25	2.212 ± 0.740	0.222 ± 0.043	1.001 ± 0.016
	19/02/2011	03/06/2011	12	2.290 ± 4.518	0.225 ± 0.271	0.990 ± 0.025
	18/01/2013	10/01/2014	207	2.004 ± 1.004	0.210 ± 0.059	0.994 ± 0.017
	19/01/2016	30/03/2016	56	2.882 ± 2.974	0.262 ± 0.175	1.006 ± 0.017
	All (original set)		260	2.011 ± 1.837	0.211 ± 0.108	0.994 ± 0.017
	All (full set)		316	2.115 ± 2.136	0.217 ± 0.126	0.997 ± 0.018

TABLE 3.1: Results for calculation of median and standard deviation Hα equivalent widths (EW), Hα Index and peak ratio (PR) for UVES and HARPS. In the UVES table all the spectra are used and the results shown by day and for all, *apart from an observation clearly consisting of noise only timed at 12/03/09 02:31:11 UTC. In the HARPS table the observations are separated where they are 300 or more days apart. In the summary lines "original set" refers to the observations up to 10/01/2014 and the "full set" also includes data from 19/01/2016 to 30/03/2016.

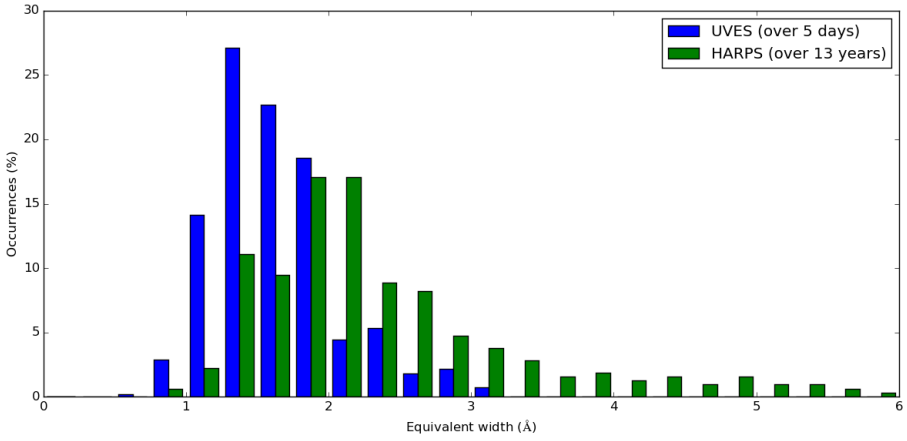

FIGURE 3.3: Histogram of equivalent widths for UVES in blue and HARPS in green with the same X axis scale. All the UVES spectra results are shown apart from those for one which appeared to be just noise (12 March 2009 UTC 02:31:11). HARPS spectra are omitted for seven outlying cases which appeared to be dominated by flares. These are listed in Table 3.3.

From	To	No.	EW	PR
27/05/2004	21/07/2004	6	1.022 ± 4.448	1.045 ± 0.028
25/07/2005	22/03/2006	5	0.243 ± 0.274	1.004 ± 0.010
14/03/2007	19/07/2007	5	0.610 ± 0.321	1.027 ± 0.009
29/06/2008	06/04/2010	25	0.699 ± 0.434	1.029 ± 0.013
19/02/2011	03/06/2011	12	0.745 ± 2.869	1.022 ± 0.023
18/01/2013	10/01/2014	207	0.579 ± 0.611	1.022 ± 0.014
19/01/2016	30/03/2016	56	1.104 ± 1.939	1.035 ± 0.017
ALL		316	0.647 ± 1.352	1.024 ± 0.016

TABLE 3.2: This table re-displays the HARPS spectra as previously shown in Table 3.1 after calculating the residual spectra from dividing by the mean values of the 5 spectra with the lowest equivalent widths. As before, the rows marked † show where equivalent widths of greater than 2 standard deviations from the median are removed and the median and standard deviations recalculated.

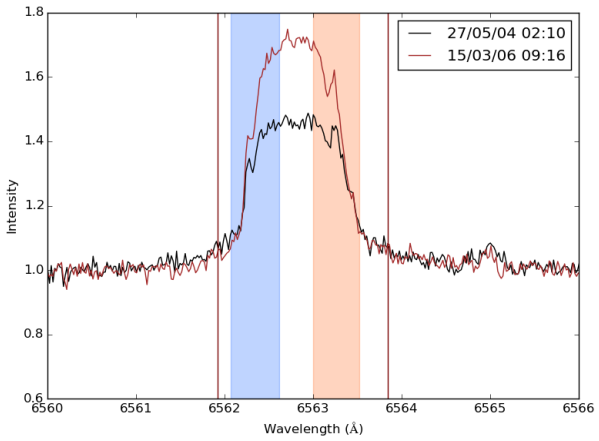

FIGURE 3.4: This figure shows the residuals of the same two spectra as previously shown in Fig. 3.1 after division by the mean of the first five spectra with minimum equivalent width timed at 16 March 2006 UTC 06:37:59, 14 March 2007 UTC 07:28:29, 5 April 2011 UTC 03:26:33, 8 April 2011 UTC 06:28:17 and 22 April 2011 UTC 05:07:46.

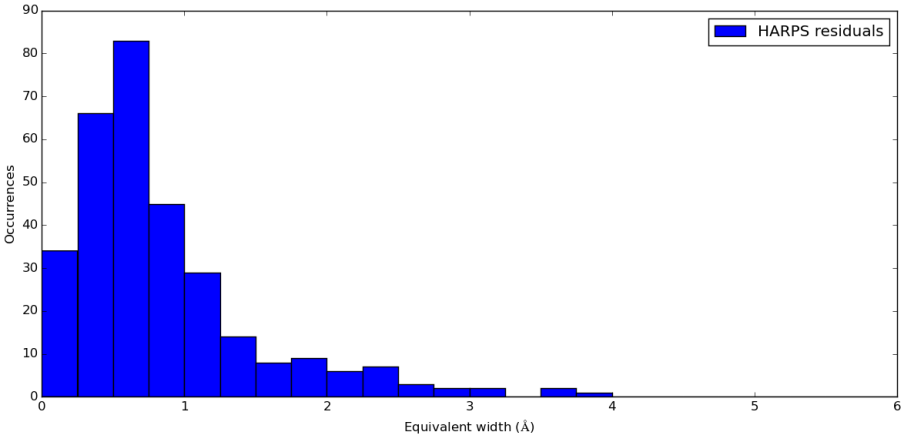

FIGURE 3.5: Histogram of the residual equivalent widths generated as for Table 3.2 and Fig. 3.4.

variations and a version of the peak ratio calculation yielded any periodicity results, albeit as stemming from the photosphere it is not a similar measure to the chromosphere as with Hα. However, no clear period could be identified, in particular the 82.6-day period could not be found in the results, which for completeness are presented in Appendix D. A similar exercise was briefly carried out with the He-6678 line in the adjacent spectral order to that for Hα used in conjunction with the flare identification in Section 3.4 but that was only prominent to any degree in conjunction with what appeared to be flares and it was not feasible to identify any periodicity in that line.

A future line of enquiry might be to combine an assortment of such lines in order to derive

a type of a composite spectral index as discussed in Hall and Lockwood (1999) and Hall and Lockwood (2000), however initial attempts to combine these lines with the Hα line proved of little value as the Hα peak is so much greater and the results were indistinguishable from the Hα results alone.

3.3 Flares in UVES data and X-ray values

In Fuhrmeister et al. (2011, fig. 1 to fig. 3) the measured flux for various wavelengths for each of the three observation nights are presented. In Fig. 3.6, Fig. 3.7 and Fig. 3.8 are displayed the Hα equivalent width and the X-ray counts for these nights together with the peak ratios. As the X-ray flux is so much greater on the third day, the third panel is potentially misleading, so these are re-displayed all to the same scale below in the bottom panel.

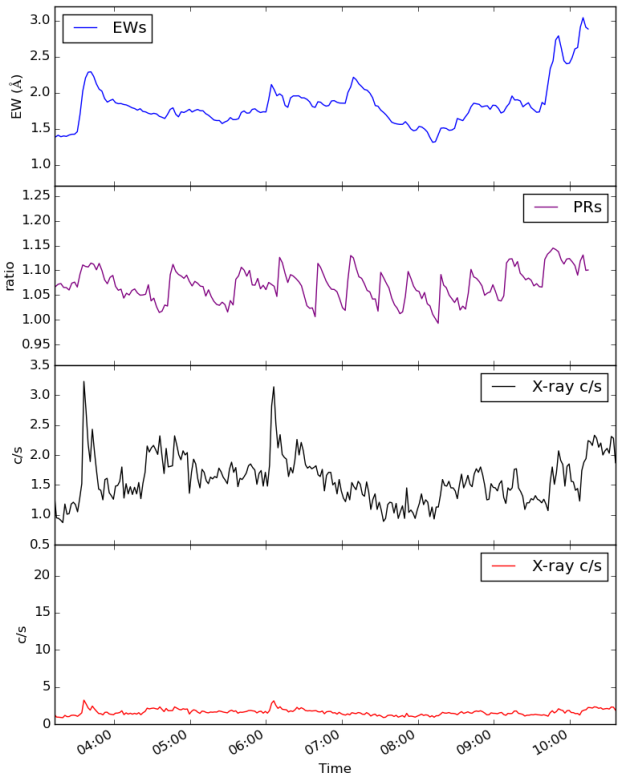

FIGURE 3.6: This plot is derived from the data from UVES on 10 March 2009. The equivalent width (top panel), peak ratio (second panel) and X-ray data (third and bottom panels) of the Hα flux as shown in Fuhrmeister et al. (2011, Fig. 1). The top two panels are on the same scale throughout. The X-rays displayed are-displayed to the same scale on the fourth panel as for Fig. 3.7 and Fig. 3.8

In Fig. 3.6 it is apparent that the peak ratios for the first day (10 March 2009) seemed to have periodic nature for a portion of the plot, as did a much smaller portion of the plot for the third

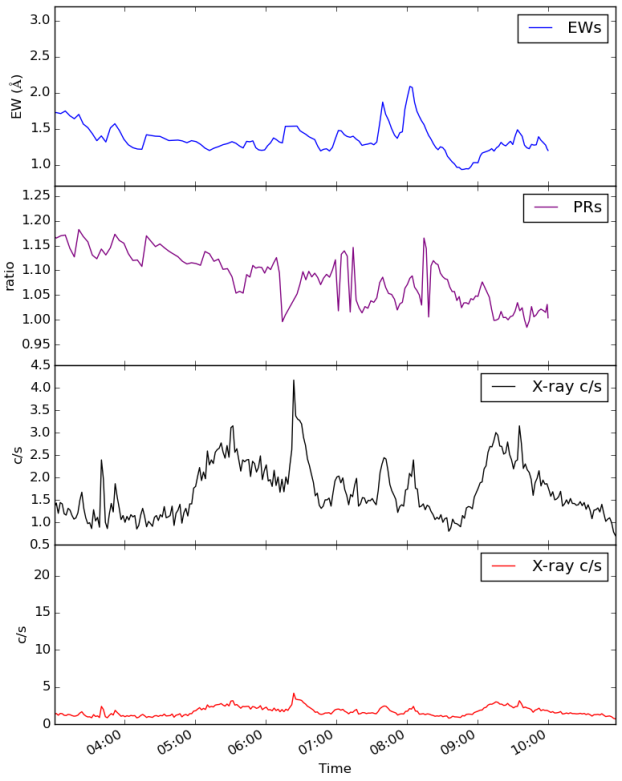

FIGURE 3.7: This plot is derived from the data from UVES on 12 March 2009. The equivalent width (top panel), peak ratio (second panel) and X-ray data (third and bottom panels) of the Hα flux as shown in Fuhrmeister et al. (2011, Fig. 1). The top two panels are on the same scale throughout. The X-rays displayed are-displayed to the same scale on the fourth panel as for Fig. 3.6 and Fig. 3.8

day (14 March 2009), shown in Fig. 3.8. The portion on the first day had a strong period of approximately half an hour and the third day a much weaker period of about 20 minutes. However there were no other periods found in the other day of a similar strength or value, either for peak ratios or equivalent widths. However it was noted that in Barnes et al. (2014, Section 4.1) there is speculation of instrumentation error on the first and third days applied to this data. By cross-correlation using the 6565-6585Å region, it is possible to shift the spectra to compensate for apparent radial velocity variations. This enables the periodic signal to be reduced substantially in the first day's plot and almost completely in the third day's plot. As these periods were not directly relevant to this project, focusing on the rotation period of Proxima Centauri which was believed to be much greater, it was decided not to investigate this particular possible behaviour further.

The UVES data showed a large flare during the third of the observation periods starting at approximately 06:15 on 14th March 2009. Both the equivalent width and X-ray counts rapidly reached a peak, with the equivalent width peaking approximately a minute before the X-ray

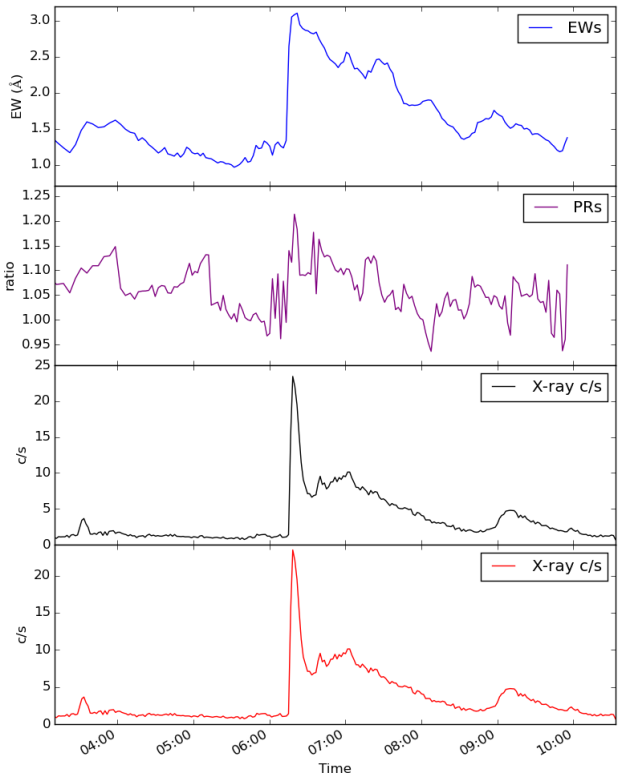

FIGURE 3.8: This plot is derived from the data from UVES on 14 March 2009. The equivalent width (top panel), peak ratio (second panel) and X-ray data (third and bottom panels) of the Hα flux as shown in Fuhrmeister et al. (2011, Fig. 1). The top two panels are on the same scale throughout. The X-rays displayed are-displayed to the same scale on the fourth panel as for Fig. 3.6 and Fig. 3.7

count peaked. The equivalent width reached a similar level at the end of the first observation period to that which it reached during the flare in the third, albeit much more slowly, but with only very slight evidence of a corresponding increase in the X-ray count. However there was an increase in the UVES optical "blue" flux on the first day, as shown in Fuhrmeister et al. (2011, fig. 1) corresponding to the higher equivalent widths, suggestive of some other process than that in the third day which did show the higher X-ray level.

3.4 Possible flares on HARPS

There are no corresponding X-ray data available for the HARPS data, but as the UVES data suggests that Hα equivalent width increases with flares, the higher values of equivalent width in the HARPS data as were selected as indicative of flares. After some experimentation with investigation of periodicity, the effects of possible flares seemed to be minimised if the proportion of data with the lower 90% of equivalent widths were selected. In both UVES and HARPS this was

approximately one standard deviation from the median, 2.0Å in the case of UVES and 4.2Å in the case of HARPS.

The HARPS data contains seven spectra with particularly large values of equivalent width of over 6.0Å, listed in Table 3.3. Following Fuhrmeister et al. (2008, fig. 8) in relation to flares on CN Leonis, the He-6678 line equivalent widths were also calculated and are also included in that table. It was noticeable that only a few spectra had any significant He-6678 emission, only seven spectra had equivalent widths greater than one standard deviation of 0.059 above the median of 0.054, which are listed in the table. If these are clipped from the He-6678 results, the standard deviation of the He-6678 line equivalent widths sinks to 0.10. In Fig. 3.9, Fig. 3.10 and Fig. 3.11 the equivalent widths for Hα and He-6678 are plotted against each other for each of the three years 2013, 2014 and 2016, showing the correlation only when the Hα line is maximal.

Epoch	EW	He-6678
18/03/2016 UTC 08:59:02	23.991	0.853
16/07/2004 UTC 01:52:40	21.693	0.312
27/03/2011 UTC 05:20:09	18.123	0.591
31/01/2016 UTC 08:51:35	7.298	*0.099
26/02/2016 UTC 09:07:05	6.898	*0.110
05/05/2013 UTC 03:31:16	6.756	0.276
05/05/2013 UTC 03:41:47	6.192	0.177
14/05/2013 UTC 06:07:49	†5.425	0.115
05/05/2013 UTC 03:53:13	†5.786	0.114

TABLE 3.3: This table lists, in descending order of Hα equivalent width, the seven spectra mentioned in Section 3.2 and Fig. 3.3 as having equivalent widths over 6.0 (and not displayed in that figure). As well as showing the values of the Hα equivalent width, that of the He-6678 line is also displayed. This table also shows the seven spectra having the He-6678 line with the largest equivalent width, five of which, not marked with * or †, are common to the set of seven with largest Hα. The two remaining out of the seven with exceptional Hα but not an exceptional He line are marked with * and vice versa for the ones marked with †.

3.5 Recovery of periods from HARPS data

Attempts to derive periodograms from the results of the the various measures listed in Section 3.2 met with much less success than the photometric results from ASAS and HST, in that, as discussed in Appendix C, all the various Lomb-Scargle routines gave very different results for almost every line measure or combination of measures. A full list of results is not listed in this report, however the overall performance is illustrated in Fig. 3.17 and Fig. 3.18 in Section 3.6. The *Numerical Recipes* routine usually failed to find periods close to the 82.6 day period identified in the photometric results or on the occasions when it found it, gave a FAP at or very close to 1.0.

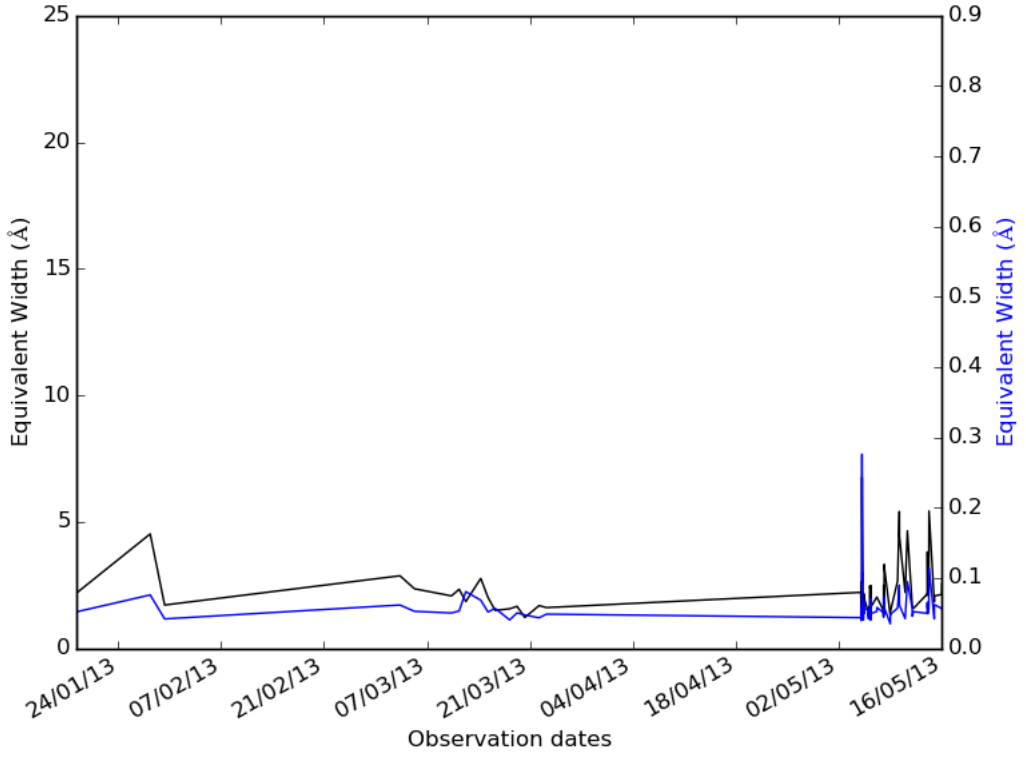

FIGURE 3.9: This plots show the Hα equivalent width in black and the He-6678 equivalent widths in blue for the HARPS observations during 2013. Vertical scales for Hα and for He-6678 are the same as in Fig. 3.10 and Fig. 3.11.

To examine the performance as well as possible, all the three Python routines described in Appendix C were tried with every set of data and the results compared. None of the routines gave any meaningful results for periods below 40 days, with a plethora of strong peaks down to fractions of a day, or above 120 to 130 days, so all the periodograms were generated with periods between 40 and 130 days, in steps of 0.01 days (14 minutes, 20 seconds). This encompassed the 41.3 days of Benedict et al. (1993), although this looks very likely to be a half-period sub-harmonic, through to and including the 116.6 days of Suárez Mascareño et al. (2015, Table 3) and encompassing the minimum period of 50 days given by Kürster et al. (1999) and the 82 days of Benedict et al. 1992, 1998; Kiraga and Stepien 2007. The erratic behaviour of the periodograms below about 40 days made it impractical to extend the search down to include the 31.5 days of Guinan and Morgan (1996), but in the light of the photometric results and the unanimity of other reports as to the period being longer than this, this was deemed not to matter.

Many of the periodograms showed several strong peaks all over the range searched, typically with up to five outstanding peaks in the range searched, so for this report note was taken of the periods of the strongest peaks and of the five strongest peaks in the analyses of the periodograms.

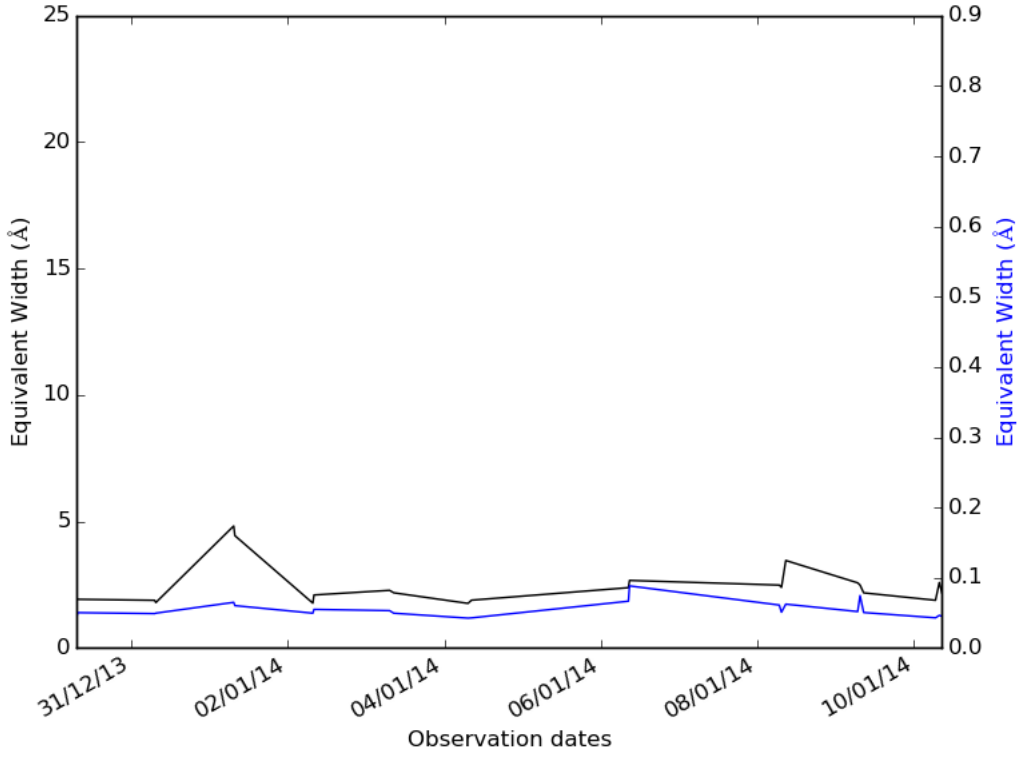

FIGURE 3.10: This plots show the Hα equivalent width in black and the He-6678 equivalent widths in blue for the HARPS observations during 2014. Vertical scales for Hα and for He-6678 are the same as in Fig. 3.9 and Fig. 3.11.

In Fig. 3.12 is shown how the different routines give different results with identical data; the upper panel showing the results from the ASTROML routine and the lower panel showing the results from GATSPY. In Fig. 3.13 is shown a result from peak ratio calculation giving a value of 82.2 days returned by GATSPY.

Some efforts were made to remove data contaminated from flares, either by clipping spectra with various upper bounds of equivalent width, by binning data or both. Following the lead from UVES in Section 3.3, spectra were clipped where the equivalent width exceeded one standard deviation from the median. This was 3.8Å for the Original Set or 4.2Å for the Full Set of data. However the latter, which included some spectra with very large equivalent widths taken in 2016, did not yield any particular benefit, so with the Full Set of data, clipping to a maximum equivalent width of 3.8Å in line with the Original Set was tried. Binning to various fractions of a day up to one day was attempted. Nothing was observed to improve the performance of any of the measurements in any consistent way, with the possible exception of peak ratios, which appeared to improve very slightly if binned to around 1 day. The results from the Hα Index were virtually identical to those from the equivalent width measure, so these are not considered

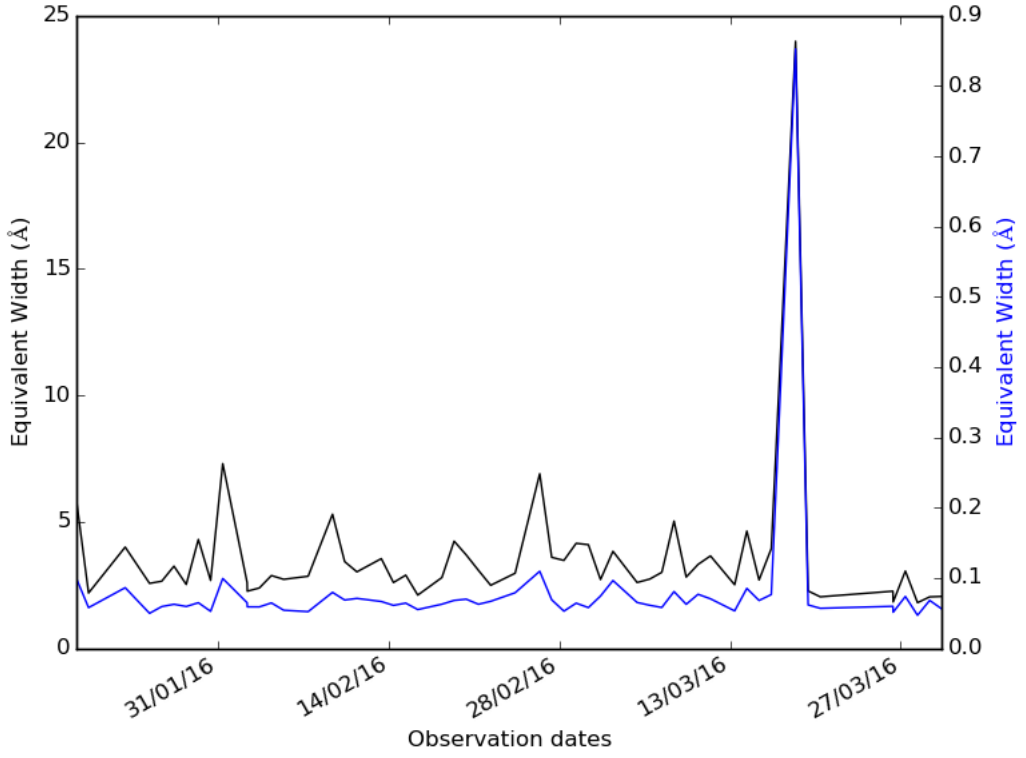

FIGURE 3.11: This plots show the Hα equivalent width in black and the He-6678 equivalent widths in blue for the HARPS observations during 2015. Vertical scales for Hα and for He-6678 are the same as in Fig. 3.9 and Fig. 3.10.

separately. The overall performance of the four methods is summarised and illustrated in Fig. 3.17 and Fig. 3.18.

With the Original Set of data, all the measurements, except for the peak ratio, returned the 116.6-day period reported in Suárez Mascareño et al. (2015, Table 3). This completely disappeared if any clipping or binning was done or the Full Set of data was examined. The window function of both these sets of observation times was examined, using *Period04* and the results displayed in Fig. 3.14 and Fig. 3.15. It was not considered that any useful conclusions could be made from these as there were so many peaks in the results.

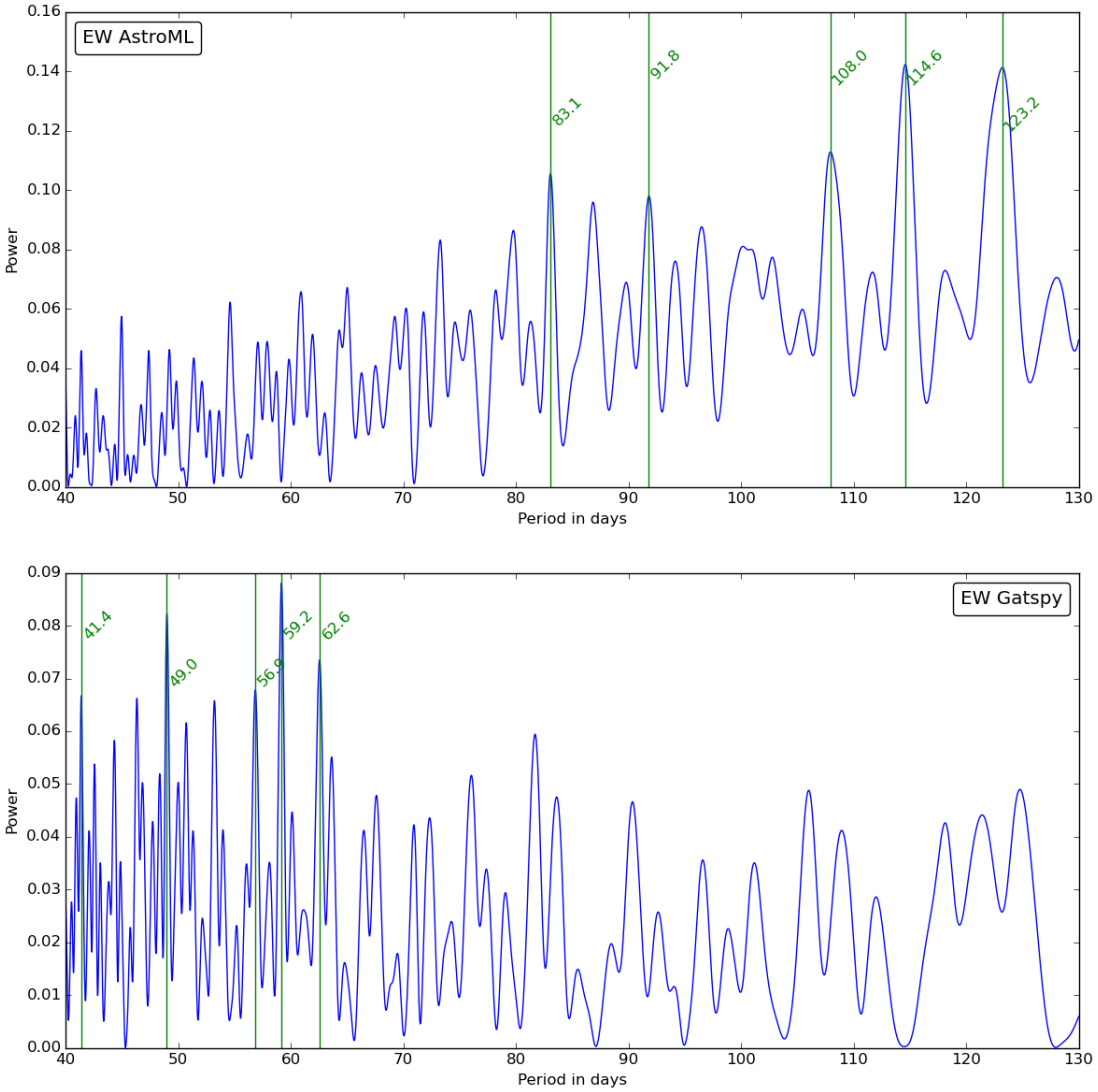

FIGURE 3.12: This figure shows sample periodograms from the Hα peak of the HARPS data, calculating from equivalent widths using ASTROML for the upper panel and GATSPY for the lower panel. The strongest 5 peaks are highlighted in both cases.

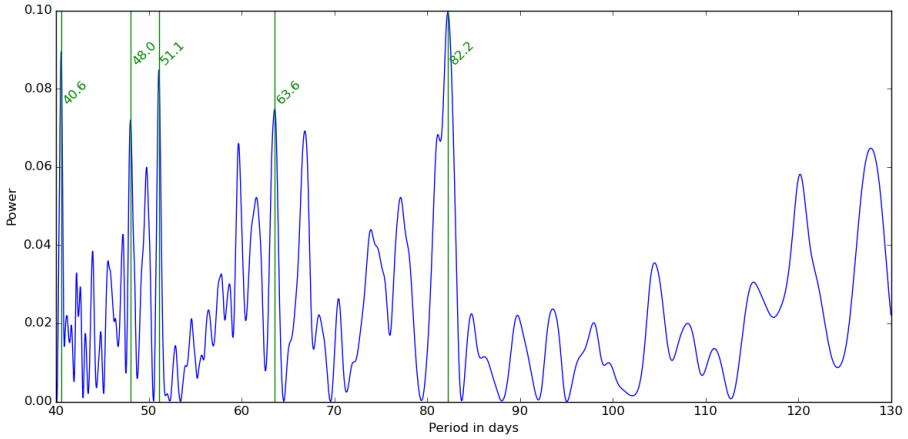

FIGURE 3.13: This figure shows a sample periodogram from the peak ratio measure from the Full Set of the data from HARPS binned to 1 day, processed by the GATSPY routine and displayed with the five highest peaks highlighted and showing the values.

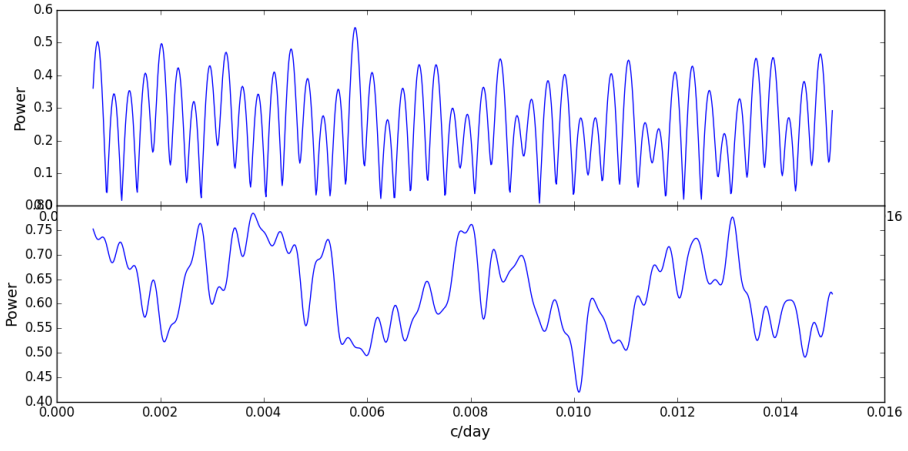

FIGURE 3.14: In the upper panel is shown the periodogram, displayed in cycles/day, of the equivalent widths from the Original Set of the HARPS data, calculated using *Period04*. In the lower panel is shown the corresponding window function.

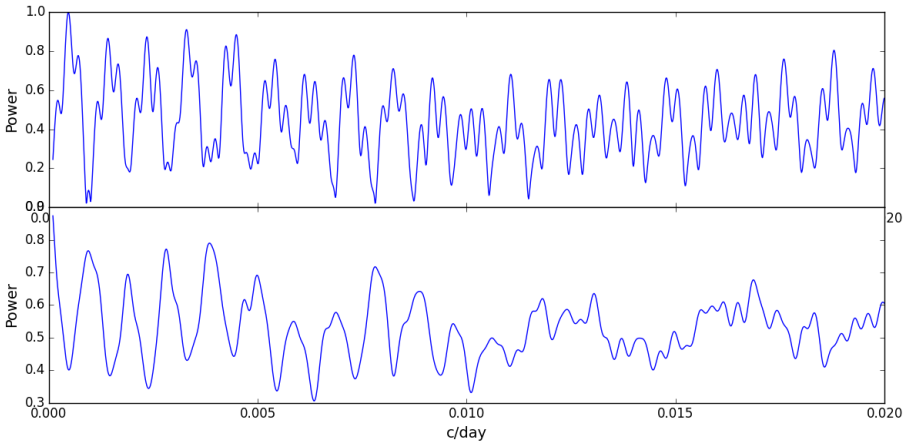

FIGURE 3.15: In the upper panel is shown the periodogram, displayed in cycles/day, of the equivalent widths from the Full Set of the HARPS data, calculated using *Period04*. In the lower panel is shown the corresponding window function.

3.6 Comparison of ASAS and HARPS for period recovery

It seemed appropriate to look in more detail at the ASAS data which offers a similar sampling cycle, based upon ground-based observations, to that from the HARPS data discussed in Section 3.5 above. Of particular importance is the False Alarm Probability for periods recovered from the spectroscopic data as well as estimating the uncertainty level of all of the calculated periods, particularly those in the photometric data. None of the three Python routines directly return an FAP and the the *Numerical Recipes* routine always returns an FAP of 1 for the periods if the periods were found at all. Consequently a Monte Carlo method was devised and implemented to study this and at the same time help estimate the uncertainty on the period obtained from the ASAS results.

The ASAS data has many more observations than the spectroscopic data from HARPS. The former has 970 and the latter has 316 (or 260 in the Original Set). If the ASAS data is binned, then as noted in Section 2.1, the number of observations becomes 924 if binned to the most optimal 18 minutes or 624 if binned to 1 day, more akin to the binning used in many of the periodicity calculations for the HARPS data, with a more comparable number of observations.

So, starting from the ASAS data, binned to 1 day and assuming for the purpose that the 82.6 day period obtained from the full set as described in Section 2.1 is correct, various percentage-sized subsets of the data were randomly selected, recalculating the periods, noting whether a value close to the correct period was recovered as the strongest peak, within the five strongest peaks, or not at all. If the period was recovered, the RMS error, assessed as the difference from 82.6 days, was recorded. The sizes of the subsets were taken between 5% and 95% in steps of 5%. For each percentage sized subset, the process was repeated 2,000 times. The results are illustrated in Fig. 3.16.

Four results are shown in Fig. 3.16. In all cases, the X-axis displays the percentage sized subset of the binned ASAS data which was used. On the left Y-axis is shown the percentage of recovery (i.e. 100% minus the FAP) of the correct period. The blue line shows the percentage recovery of the correct period as the strongest peak with various percentage sized subsets of the data and the green line shows the percentage recovery of the correct period as one of the five strongest peaks, not necessarily as the strongest peak. If can be seen that the former reaches 100% recovery at about 70% and the latter at about 45%.

On the right Y-axis is shown the RMS error in the period when it is recovered correctly. The purple line shows the RMS error in the results corresponding to the case where the correct period is recovered as the strongest peak and the red line the RMS error in the results corresponding to the case where the correct result is found in one of the top five peaks. It is noticeable that this reaches less than 0.1 days in both cases, lending weight to the conclusion that the uncertainty in the 82.6 peak found by ASAS and HST is of the order of 0.1 days at worst.

Finally, marked in as the dotted vertical black lines are the percentages where various numbers of observations with various clippings and binnings of the HARPS data would come. The actual numbers of observations range from 55, or 8.8% of 624, to 316, or 50.6% of 624. The intersections with the blue lines would indicate the level of FAP which would be expected from the most powerful peak in the corresponding periodogram and that with the green lines would indicate the level of FAP as one of the top five peaks.

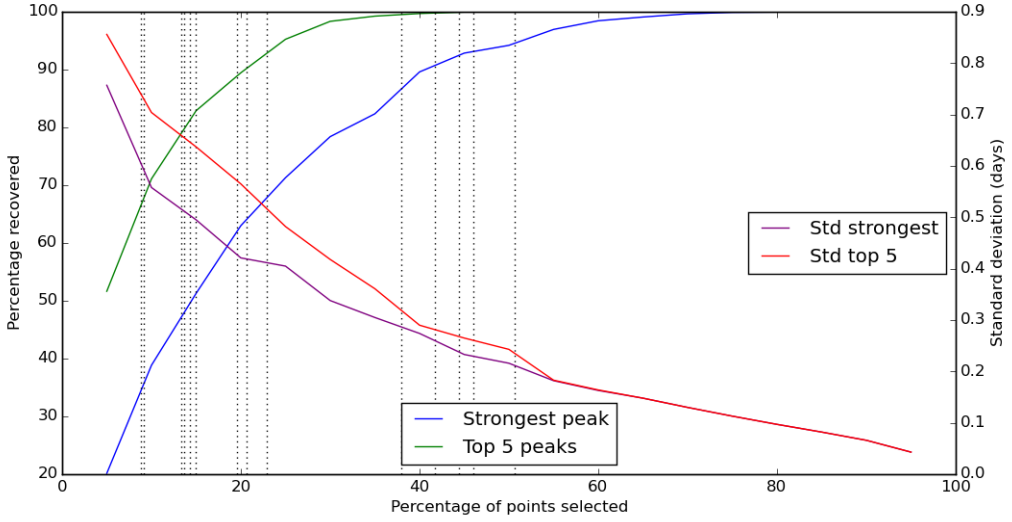

FIGURE 3.16: In this figure is illustrated the effects of randomly selecting a given proportion of the ASAS data in terms of whether the same period of 82.6 days is recovered and the error in this result. The black vertical dotted lines mark in the proportions of data corresponding to the number of observations remaining in the HARPS data after various clippings and binnings have been performed.

3.7 Performance summary of spectroscopic measurements

Having seen how the performance of the photometric results is affected by the reduction in the number of points to those it is useful to compare the variants of spectroscopic measurements

against these to assess the reliability of each of those. To do this, all of the results of the four measurements studied in this report, after all variants and combinations of clipping and binning were collated together. In Fig. 3.17 is shown the comparisons of each of these methods against the "worst case" of the subset of ASAS results shown in Fig. 3.16. In this figure, the blue bars indicate where each of the measurements return 82.6 days to within 0.5%. (This level of acceptability corresponded approximately to the standard deviation of the "worst case" of the ASAS results as shown in Fig. 3.16.) It was noticeable that a good number of the results returned the likely sub-harmonic of 41.3 days (as given in Benedict et al. (1993) so the yellow bars illustrate this. It is clear that the peak ratio measurement is much the best, whilst the skewness measurement never returns the 82.6 day period at all. However all fall well short of the ASAS results.

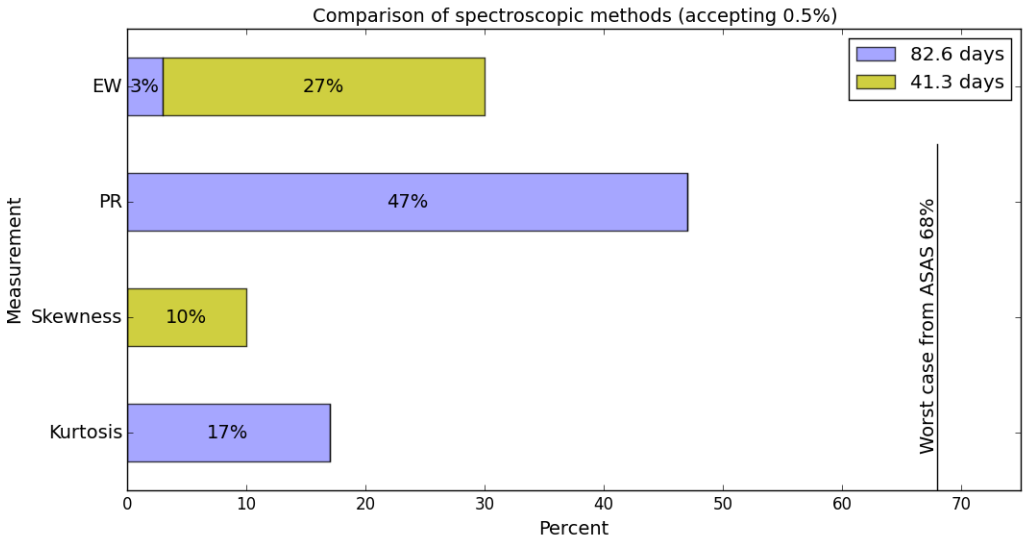

FIGURE 3.17: This figure illustrates the relative performance of each of the 4 spectroscopic methods with the Full Set of HARPS data against the "worst" instance of the restriction of the ASAS points as shown in Fig. 3.16. In all cases it is regarded as "success" to recover an 82.6 day period to within 0.5% as one of the largest five peaks of the corresponding periodogram. For each of the four spectroscopic methods considered, all variants of clipping, binning, taking residuals and appropriate combinations of those are collated, to give an overall performance for each measurement method as a percentage. Shown in blue on the spectroscopic results is the percentage to which 82.6 days is recovered. In some cases it was noticed that the 41.3-day sub-harmonic could be recovered and the additional yellow bars denote that proportion of the results in which this was noted (where 82.6 days was not also recovered).

If the threshold of acceptability is relaxed to accept results within 2%, rather more of the spectroscopic results become acceptable, as shown in Fig. 3.18. Both equivalent widths and peak ratio measurements return a period within 2% of 82.6 days half the time, with the former slightly better. It is noticeable that the skewness measure considerably improves with this tolerance.

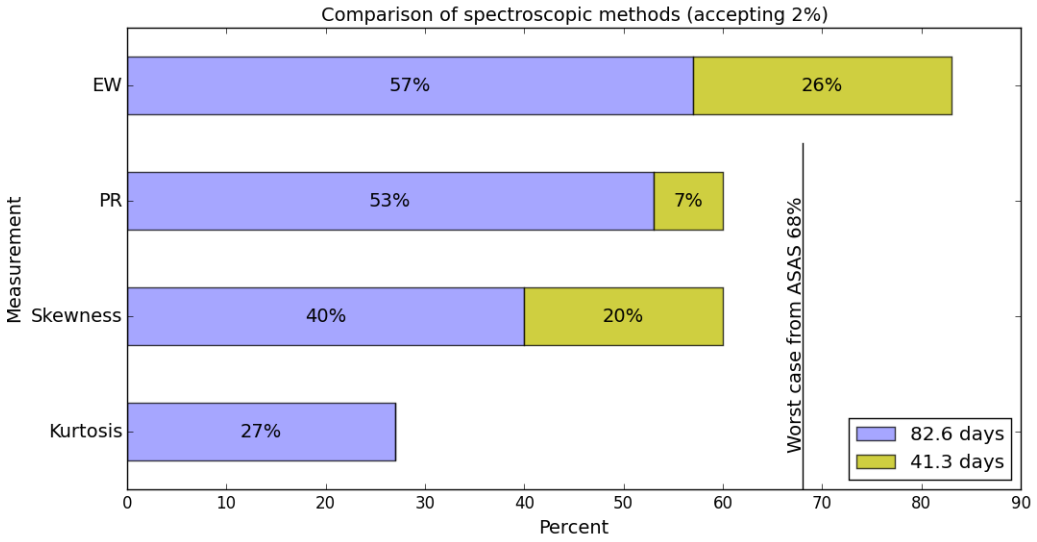

FIGURE 3.18: This figure is Fig. 3.17 reworked to illustrate the relative performance of the spectroscopic measurements if periods are regarded as valid to within 2% rather than 0.5% of 82.6 days (or 41.3 days).

The performances of these measurements was substantially worse with the Original Set of HARPS data up to 2014. With up to 0.5% tolerance the equivalent width measure found the 82.6-day period in 5% of cases as opposed to the peak ratio which found it in 38% of cases, whilst the skewness and kurtosis measurements did not find it at all. Improvement was negligible if the tolerance was increased to 2% or even 5%.

It should, of course, be emphasised that this is recovery within the strongest five peaks of the periodogram. In only a handful of cases was 82.6 days the strongest peak and those were for the peak ratio measure with 1-day binnings.

Chapter 4

Modelling of Proxima Centauri spectra

In order to develop and refine the methods for evaluation of the periodicity of the sub-peaks in the Proxima Centauri spectra, a version of the "Doppler Tomography of Stars" (DoTS) modelling software (Collier-Cameron, 2001) was used. Although DoTS was written to recover surface imhomogeneities from time series spectra, here the forward modelling routines were used to generate synthetic spectra, with some modifications. Specifically, a 3D model of the star, but with a 2D spherical model of the photosphere was constructed, covered in a finite number of pixels. The intensity of each pixel can vary from a photospheric value to a value appropriate for plage. In order to obtain the appropriate photospheric intensity for each pixel at a given rotation phase of the stellar model,the 4-parameter limb darkening law introduced by Claret from Phoenix model atmospheres (Claret, 2000) was used for an effective temperature of 3000K. The plage intensities were calculated according to Unruh et al. (1999, Section 4.1), who identified the centre to limb variability from plage regions relative to the photospheric (quiet) intensity for the Sun. Since no such observations exist for other stars, the same centre-to-limb variation as for the solar plage was used relative to the photospheric centre-to-limb variation of Proxima Centauri, selecting the limb-darkening law appropriate for the lower photosphere temperature and with appropriate facular contrasts for Hα wavelengths (see Unruh et al. (1999, figs 3 & 4)).

Since it was desired to simulate the Hα line profile, a local intensity profile was assumed for the photosphere and the plage. For inactive photospheres of M-dwarfs with similar spectral type to Proxima Centauri, Hα is not visible (e.g. see Hα profile in Barnes et al. (2014, fig. 6) for GJ1061). Hence for the quiet photosphere, a flat continuum was assumed For active

stars, Hα possesses a characteristic emission profile with self-absorption, resulting in a double-peaked profile. Since the $V_{\rm eq} \sin i$ is probably less than 0.1 km/s for Proxima Centauri, the local line profile shape for Hα was based on the observed Proxima Centauri line profile since it is unlikely to show rotational broadening. This profile was tuned to resemble the average Hα profile shown in the UVES data analysed in Fuhrmeister et al. (2011), but symmetric about the central wavelength. Specifically, a Gaussian profile was used to generate the emission peak and a second Gaussian with narrow width to represent the central self-absorption as illustrated in Fig. 4.1. The profile was selected with the spread of wavelengths in resembling the Hα peak and with equivalent width so as to resemble the mean peak in the HARPS data. The intensity could be fine-adjusted in the lookup-table parameters for the DoTS program so as to yield a variation in equivalent width comparable to that of the HARPS observations ignoring those affected by flares with the selected plage distribution in use.

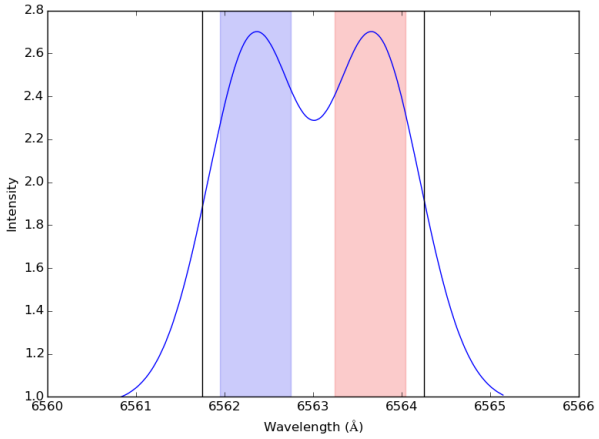

FIGURE 4.1: Example generated model spectrum of Proxima Centauri, also illustrating the methods for computing the periodicity of spectra. The centre of the Hα line is set at 6563Å for convenience rather than 6562.8Å. The green lines (from 6561.75Å to 6564.25Å) show the limits used for calculation of the equivalent width. The blue and red shaded areas (6561.95Å to 6562.75Å and 6563.44Å to 6564.24Å respectively, each 0.8Å wide) show the regions for calculation of the peak ratio.

With the two-temperature model, in subsequent simulations below, either photospheric intensity or a plage intensity is assigned to each pixel. For a pixel containing plage, the synthetic Hα profile is scaled and for the photosphere with no visible profile (as note above), the continuum level is used. The line profile is shifted appropriately for the Doppler shift of each pixel in the model, however with the small Doppler shift due to the $V_{\rm eq} \sin i$ of less than 0.1 km/s on Proxima Centauri, the main velocity variation observed is due to the asymmetry of the plage distribution. The model enables the user to place circular spots of specified radii anywhere on the star. For

each viewing angle (or equivalently observation phase), the appropriate intensity profiles of all visible pixels is calculated (according to position on the line and centre-to-limb variation) and sum them to obtain the simulated line profile.

A model star with plage regions that rotate into and out of view can thus potentially exhibit variability in the line shape since the pixels on different parts of the star possess different Doppler velocities. For stars such as Proxima Centauri, which probably possess a $V_{\rm eq} \sin i$ much less than the instrumental resolution, any velocity distortions in the the line profile due to spots rotating into and out of view will be insignificant or very small. A plage region that rotates into view may nevertheless have a significant effect on the the equivalent width of the simulated line since the local intensity profile for Hα possesses a greater normalised peak intensity than the continuum. For stars with rotational velocity much greater than the instrument resolution, line asymmetries are likely to be much more reliable.

4.1 Plage distribution and results

During the course of experimentation with models, a selection of plage distributions was tried, ranging from a single large spot on one face to randomly-placed spots of random sizes. In all cases a 100% filling factor for the plage was selected. However it was found that the variation in equivalent widths from a low spot coverage was bore no possible resemblance to that from observational data, in that the generated simulated spectra just exhibited two extremes of equivalent widths and no intermediate values. On the other hand a coverage of more than about 30% provided very limited swings in the equivalent width compared those observed from HARPS and UVES. After some experimentation, a randomly distributed plage was settled upon which covered up to 2.5% of the surface, towards the high end of the coverage of up to 2.7% reported in Guttenbrunner et al. (2014) in relation to the Sun, with the intensity parameters in the flux profile and the model adjusted to yield a variation in equivalent widths similar to the HARPS observations.

The models were all generated with the observation dates from the Original Set of HARPS[1], using possible rotation periods between 15 and 90 days in steps of 5 days and inclinations between 10°

[1] This work was completed before the 2016 data was available. Also, as discussed in Section 4.2, it proved useful to study the Original Set of data as the 116.6 day period of Suárez Mascareño et al. (2015, Table 3) appeared in some cases, as illustrated in Fig. 4.6.

and 90° in steps of 5° to observe the various effects. Only a limited selection, usually multiples of 10 days and 10° are shown in this report to conserve space.

In Fig. 4.2 some example spectra showing extremes of equivalent width and the median are shown, and in Fig. 4.3 the corresponding visible faces of the star with the plage spots marked in.

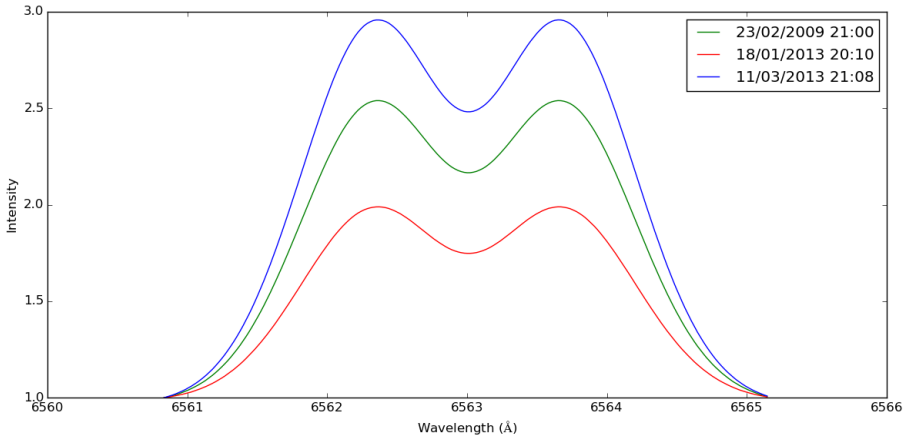

FIGURE 4.2: This displays simulated spectra showing the extremes and the median value of equivalent width (1.5, 3.0 and 2.3 respectively) with a period of 80 days and an inclination of 80°. The epochs from the HARPS data are used in the model and the selected generated spectra superimposed.

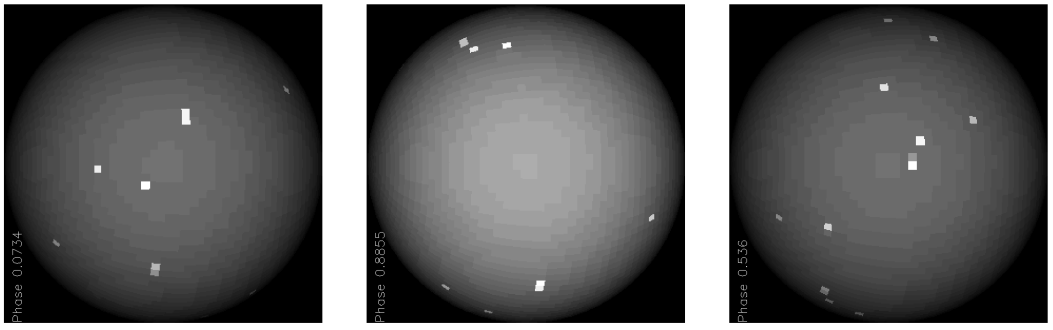

FIGURE 4.3: This shows the visible face of the star as generated by DoTS corresponding to the spectra displayed in Fig. 4.2 in chronological order. Left to right, these give the spectra with the median, the lowest and the greatest equivalent widths.

In table 4.1 are presented a selection of typical results showing means and standard deviations for the equivalent width method (EW) with the two plage distributions for various periods and

with 30°, 60° and 90° inclinations and for 70, 80 and 90-day periods with 10° to 90° inclinations. Note that the PR results are not displayed as variations were insufficient to be displayed in less than 6 figures, the Doppler variations are just too insubstantial.

Plage Dist	Period	30°	60°	90°
Random to 2.5%	20	2.150 ± 0.572	2.746 ± 0.939	2.735 ± 0.891
	30	2.725 ± 0.495	3.870 ± 0.895	4.004 ± 0.942
	40	1.917 ± 0.541	2.501 ± 0.927	2.614 ± 0.967
	50	1.604 ± 0.483	1.996 ± 0.805	2.018 ± 0.876
	60	1.626 ± 0.573	2.057 ± 0.951	2.099 ± 1.006
	70	1.967 ± 0.445	2.334 ± 0.803	2.340 ± 0.821
	80	1.637 ± 0.495	2.161 ± 0.805	2.309 ± 0.828
	90	2.475 ± 0.548	3.365 ± 0.894	3.410 ± 0.901

Plage Dist	Incl°	70 days	80 days	90 days
Random to 2.5%	10	1.693 ± 0.140	1.484 ± 0.182	1.816 ± 0.196
	20	1.811 ± 0.292	1.492 ± 0.356	2.116 ± 0.387
	30	1.967 ± 0.445	1.637 ± 0.495	2.475 ± 0.548
	40	2.116 ± 0.590	1.810 ± 0.626	2.827 ± 0.691
	50	2.237 ± 0.711	1.994 ± 0.732	3.139 ± 0.815
	60	2.334 ± 0.803	2.161 ± 0.805	3.365 ± 0.894
	70	2.392 ± 0.860	2.277 ± 0.848	3.477 ± 0.930
	80	2.396 ± 0.877	2.338 ± 0.850	3.464 ± 0.911
	90	2.340 ± 0.821	2.309 ± 0.828	3.410 ± 0.901

TABLE 4.1: Simulated mean equivalent widths with associated standard deviations from simulations for the 2.7% plage distributions and a set of rotation periods and inclinations. In the first table results are illustrated for various periods and for 30°, 60° and 90° inclinations. In the second table results are illustrated for various inclinations and 70, 80 and 90-day periods as these are close to the rotation period of Proxima Centauri.

For each set of generated spectra for both plage distributions, rotation period (between 15 and 90 days in steps of 5 and inclination (between 10° and 90° in steps of 5°), a periodogram was obtained, viewing periods between 10 days and 130 days in steps of 0.01 days, from the calculated equivalent widths and the RMS error over all inclinations noted. In nearly all cases the error was rarely more than 0.02 days. It was rather a different matter for the peak ratios however, in that the variations observed in the peak ratios were typically 2×10^{-5} at most or with the most extreme plage distributions could be stretched to 2×10^{-4}. These variations are just above the level at which it is possible to reliably measure the peak ratio from the observed data but far below the observed peak ratio changes in the data which are two orders of magnitude higher, e.g. combining all the HARPS data, a result of 0.997 ± 0.018 (one σ) was obtained.

An attempt was made to reproduce the peak ratio variations by considering an asymmetric pair of Gaussians either side of the central wavelength for the plage flux profiles, but in order to achieve the observed variations, a vertical velocity approaching 100 km/s would be required. This is well in excess of the speed of sound in the chromosphere, estimated for the Sun as approximately 8 km/s (Uitenbroek, 2004) and would therefore have to be discounted as unphysical.

4.2 Adding in noise and flares

Despite the limitations of the simplistic model, some confidence could be expressed in the measurement of periodicity from the equivalent width method, although the peak ratio variations could not be reproduced from a straightforward model and that method reliably applied. These results are for a noiseless set of models and to compare with reality the performance of the modelling results and the analysis methods in the presence of observational noise and also the influence of simulated flare events has to be considered.

As a first step in moving to something like actual observational data, noise of a given signal to noise ratio was added to the simulated spectra and the effect observed on the accuracy of the periodicity measurements for various levels, inclinations and starting periods. Adding Gaussian noise with SNRs from 100 down to 1 in steps of 0.1 was tried. These were tried with all the combinations of inclinations and starting periods tried before and attempts made to see how that affected the rate of recovery.

It was noticeable that doing this only started to have any significant effect with SNR below 20. Below this level, two things started to happen, increasingly as the SNR was reduced. Either the error in the recovered period increased, although not by very much (typically less than 2%), alternatively the recovered period was manifestly incorrect, giving a clear False Positive such as returning a period of 50 days from a starting period of 80 days.

It was easy to discriminate between these two cases by setting a threshold of 5% for the difference between the recovered period and the starting period. If the difference exceeded this, then the period was regarded as incorrectly recovered, otherwise it was regarded as correctly recovered but with the given error. However in all the cases the difference was either substantially greater or substantially less than this.

Also examined was the possible effect of flares. The effect of flares was simulated by taking the spectra which were clipped as having excessive equivalent width in Section 3.5[2] and adding in the same proportionate excess over the median equivalent width in the model as was found in the observed data. The result was a poorer performance than with noise alone, but not by much. With just noise, the performance became markedly low with a SNR of 15 or below but adding flares as described significantly reduced the performance with a SNR of 20 or below. These

[2]N.B. This was done with the Original Set of data and observation times as previously noted.

values of SNR are much lower than the published values for UVES and HARPS, which are in both cases well over 200[3].

In Fig. 4.4 is shown the effect of varying SNR and adding in simulated flare data on the rate of recovery, expressed as a percentage of the correct period of 80 days. Each data point was calculated 100 times with different randomly-generated noise[4]. The blue plot shows the effect of just adding noise, the green that of adding in the four largest flares and noise and the red shows the effect of adding simulated flares from all the values in the HARPS data clipped having equivalent width over 3.8. This is illustrated for inclinations of 30°, 60° and 90°. it can be seen that the smaller inclinations have a significantly deleterious effect on the rate of recovery especially in the presence of flares.

It should be stressed that this is the rate of recovery of the correct period as the strongest peak in the periodograms, not as one of the top 5 as in, for example, Fig. 3.17. All of the models apart from a few from the very poorest SNRs of less than 5 at low inclination gave the correct period as one of the top five peaks.

It was of interest to note the impact of the rotation period on these results, in Fig. 4.5 is shown effectively the same data as Fig. 4.4, but with a period of 60 days instead of 80 days. It was noticeable how this performed significantly better than the 80-day period, closer to the 82.6-day period calculated for Proxima Centauri. Further reductions in the period improved the recovery still further, in a relationship apparently better than linear (although many more simulations, in terms of numbers of runs and length of periods, would be required to establish this with accuracy), lending weight to the contention that the spectroscopic line measurements are likely to prove of more value with stars with a faster rotation period than Proxima Centauri.

Some of the false positives from these simulations were noted and in quite a few cases it was noticed that periods close to 116.6 days reported in Suárez Mascareño et al. (2015, Table 3) appeared as one of the prominent peaks in the modelling results. An example is shown in Fig. 4.6. This period is clearly an artefact of the observation times, which were copied from the Original Set of HARPS data for use in the model, although it was not possible to confirm this from the window function of the data, as shown in Fig. 3.14.

[3]The calculations of equivalent width, Hα Index and peak ratios for HARPS also calculated the uncertainty in the these values, which remained of the same order.

[4]For an exhaustive analysis this would clearly have to be repeated many more times, but 100 times seemed adequate for an overview.

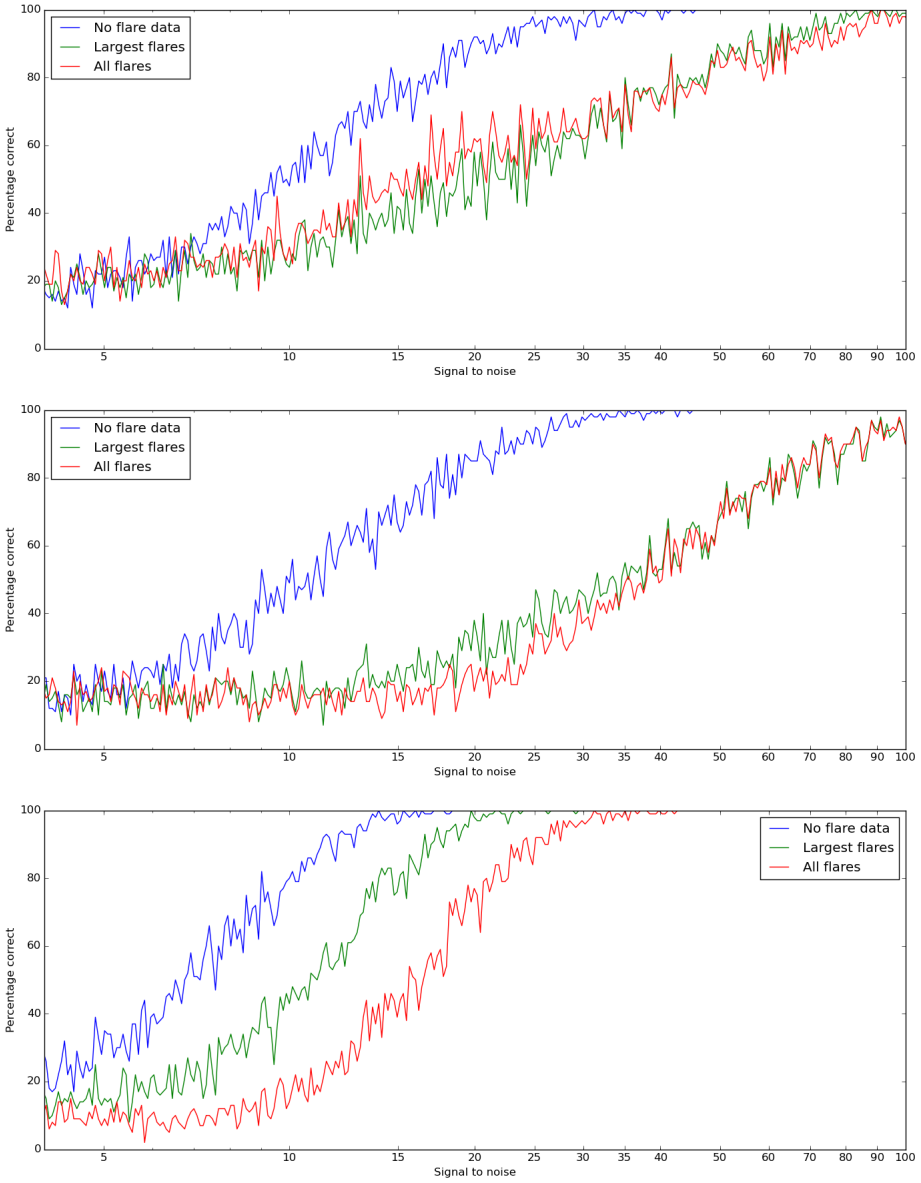

FIGURE 4.4: This figure shows the percentage of the correctly recovered period of 80 days as the strongest peak with various levels of SNR and adding various levels of simulated flare data, the blue plot for no flare data. the green plot with the four largest flare data (up to the January 2014) and the red plot the flare data clipped in Section 3.5 as having equivalent width greater than 1 standard deviation from the median in the original data to January 2014. The topmost panel shows the results for an inclination of 30°, the middle panel that for 60° and the bottom panel for 90°.

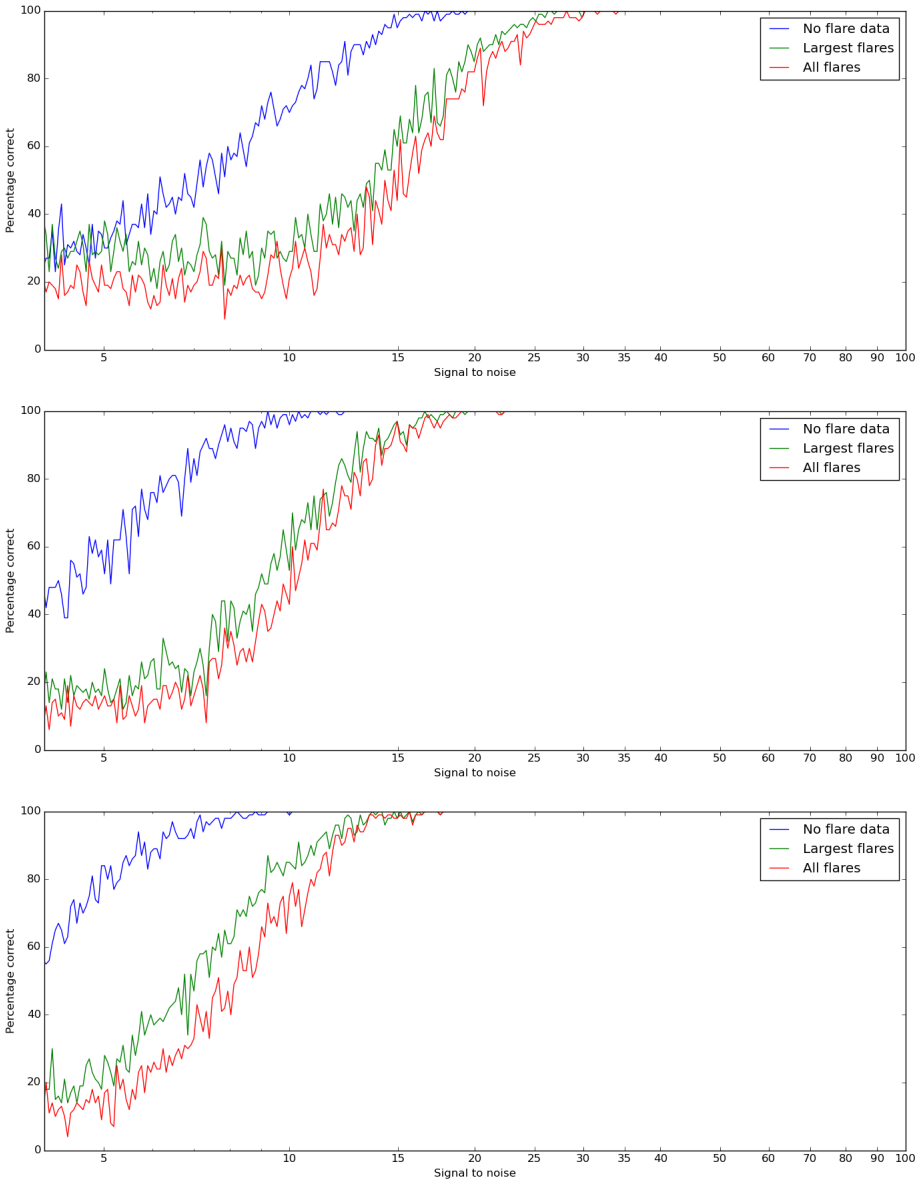

FIGURE 4.5: This figure is effectively the same as Fig. 4.4, but from a starting period of 60 rather than 80 days, showing the significant improvement in the recovery rates with the shorter period.

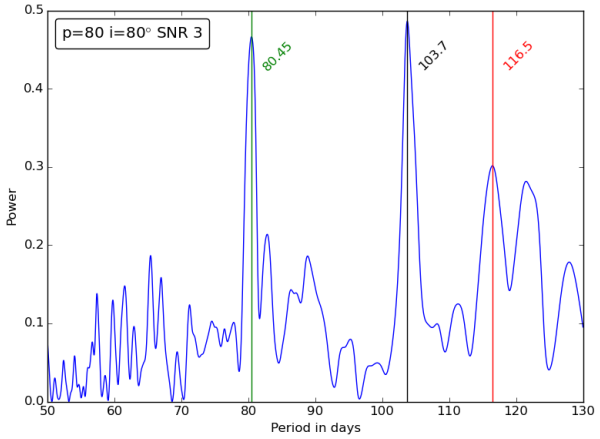

FIGURE 4.6: Example of a periodogram from the modelling simulations after adding noise which returns a peak close to 116.6 days.This was from a case where no flare data was added, to a model based on a period of 80 days, an inclination given of 80° and a SNR of 3. Here 116.5 days appears as the third-strongest peak (highlighted in red). This example gives the strongest peak as 103.7 days, marked in black and the correct period as 80.45 days, marked in green.

Chapter 5

Discussion

It is clear that the period of 82.6 $\pm$ 0.1 days given by the photometric results for ASAS and confirmed by HST in Chapter 2 must be the rotation period of Proxima Centauri, in line with Benedict et al. (1998) and confirmed by Kiraga and Stepien (2007). The sub-harmonic of 41.3 days was checked for, and indeed appeared in some of the spectroscopic results, but this was not nearly as strong. It was a similar story for double the period of around 165.2 days. There was a near-zero FAP value against 82.6 days and all the Lomb-Scargle routines which were tried gave exactly the same result with identical periodograms (apart from allowances for scaling of the power which differed between the routines). The experiments in Section 3.6 with taking subsets of the data and noting the changes in FAP and the standard deviation of the error, with only limited extrapolation of the chart in Fig. 3.16, give confidence in assigning the error bar on this period as being no more than 0.1 days.

It was not possible to obtain as clear-cut results from spectroscopic methods involving analysis of the Hα peak of the Proxima Centauri spectra, in terms of returning the period at all, obtaining a clear-cut topmost peak in the periodograms or obtaining a reasonable error bar. As can be seen in the summary in Section 3.7, the peak ratio method appears to perform significantly better, in terms of the error bar and rate of recovery of the correct period, than the equivalent width method, with skewness and kurtosis methods of possible value, but rather worse in terms of accuracy. The results are of the same kind of order as the performance illustrated in Fig. 3.16, for similar numbers of observations, but clearly cannot be used, standing alone, to compute the rotation period. Clipping high equivalent width observations, or binning to various periods can improve some results, but not in any consistent way and only seem to have an effect on

equivalent width and peak ratio measurements, not with skewness and kurtosis measurements, to which these made little difference.

There is also a strong peak of 106.3 $\pm$ 0.1 days on the ASAS results and seen in some of the spectroscopic results and the modelling, but not seen in the HST results. This period would appear to be a "beat" between the rotation period and an Earth year, which would not affect the HST results, which are far less constrained by the time of year. This is further confirmed by the consideration of the window function, illustrated in Fig. 2.3. There is also a strong peak of 77.8 days on the HST results which is not seen in the other results, but this appears likewise to be an alias with the window function.

It has proved possible to reproduce the 116.6 days of Suárez Mascareño et al. (2015, Table 3) in both the treatments of equivalent width and Hα Index and in some of the other variants of the handling of those, together with periodograms taken from the skewness and kurtosis. However, this peak is the fifth strongest in the periodograms if the period search is extended to 40 days and disappears if any kind of selection or binning is made from the data or if additional data from 2016 is included. In addition, it was noticed that some of the modelling results (see Section 4.2) also gave periods close to 116.6 days from the same observation times as in the HARPS data. From this analysis, this would clearly have to be discounted as a false positive, almost certainly an artefact of the observation times.

Limiting the portion of the spectrum examined to just the Hα line of Proxima Centauri, even with the instrumental stability of HARPS was proven to be less useful than ASAS ground-based photometry for the recovery of period. As a possible future line of investigation to be considered for some stars is that of combining fluxes from various magnetic/activity sensitive lines in various spectral orders to re-evaluate the Composite Spectral Index referred to in Hall and Lockwood (1999) and Hall and Lockwood (2000), but this would be unlikely to be effective for Proxima Centauri with its low rotational modulation. This was very briefly explored in the context of the examination of the TiO line and the He-6678 lines described in Appendix D, with no encouraging results at all, confirming the likely in-applicability of such a technique to Proxima Centauri.

It was possible to reproduce the variations in equivalent width seen in Proxima Centauri using the DoTS model and show that the recovery of the rotation period has validity. However, even with extensive experimentation, including relatively extreme values for the various parameters for limb-darkening and contrast or extreme distributions of plage, it was not possible to model

the observed variations in peak ratio found either in the UVES or HARPS data with a symmetric flux profile. It is clear that the variations in the two sub-peaks that are purely due to Doppler shift from the rotational velocity are not large; with a radius of 0.141 Solar (Demory et al., 2009) and assuming a period of the order of 80 days the rotational velocity is at most 90 m/s yielding a Doppler shift of at most 0.003Å in the Hα line between the extremes of the disk and the centre, far too low to reproduce the variations in the Hα line profile as as illustrated in Fig. 3.1 for which the peak ratios were calculated as 0.997 ± 0.018 (see Table 3.1). The best standard deviation on a peak ratio close to 1.0 which could be obtained from the models was 2×10^{-5} or 2×10^{-4} with very extreme plage distributions. This was not surprising due to the lack of Doppler broadening of the line profile.

What was clear from the models was the way in which period recovery was adversely affected by the inclination and improved as the rotation period was decreased, this is demonstrated by the results obtained in Section 4.2 and samples shown in Fig. 4.4 and Fig. 4.5. This at least suggests that deducing the rotation period by photometric measurements may become increasingly feasible for faster rotating stars. The spot and plage configurations are likely to change less between successive rotations with a faster rotating star, so this will also increase the probable accuracy of calculations relying upon these.

It is probably naive to expect the plage configurations to be comparatively unchanged over such a long rotation period as that for Proxima Centauri and basing the models on this assumption is unlikely to reflect the observed variations correctly. More importantly, it is also clear that the model of static plage and spots supported by DoTS cannot accurately reproduce the observed variations in the peak ratios. Likewise it cannot reproduce the range of phenomena which adversely affects obtaining periodicity from the equivalent widths.

Experimenting with adding the effect of a net vertical velocity to the flux profiles to the DoTS model showed some improvement in the variation of the peak ratios, but as noted above, this would be an unphysical velocity component and has to be discounted. Also doing this does not adversely effect the equivalent width measure as found in the observational data. This points to the need for a properly-constructed 3D model, taking into account activity in the chromosphere and corona other than those close to the photosphere and not possible to model with a simple spherical shell, to properly understand the behaviour of Proxima Centauri.

In the literature, similar conclusions are reached by Rauscher and Marcy (2006) as an explanation for H, K and Ca line asymmetry, however these were for earlier type of stars than Proxima

Centauri, of type K7 to M5, for which Hα is in absorption. The sub-peaks shown in fig. 2 in that paper have the red sub-peak smaller than the blue sub-peak as opposed to Proxima Centauri as shown in Fig. 3.1, for which it is in most cases the other way round. The authors suggest that this effect is caused by slowly-decelerating motion toward the observer which does not fall back ballistically away from the observer which would therefore be blue-shifted and hence enhance the blue sub-peak. With Proxima Centauri, it might be a similar effect is taking place but the self-absorption portion is blue-shifted which would be inverted to resemble a red shift.

Chapter 6

Conclusions

This report has set out to study measurements of periodicity via measurements of the Hα line in particular and focusing on Proxima Centauri.

A study of photometric measurements from ASAS and HST produced clear evidence of a rotation period of 82.6 ± 0.1 days with negligible FAP. This produced a benchmark from which to evaluate spectroscopic measurements including that of equivalent width and the virtually identical Hα Index, which were applied to the Hα line to demonstrate that they did not prove able, in terms of reliable recovery of the period at all or with an acceptable error bar, to deliver a result in isolation, certainly as far as Proxima Centauri is concerned. The measurement of lines presented in this report, the peak ratio, appears to be consistently better than other measurements and is particularly suitable for Hα line profiles such as that for Proxima Centauri, which have a "horned" appearance with two sub-peaks around a relatively unchanging central minimum.

A look at simple 2D models enabled the variations of equivalent widths to be reproduced and the validity of the methods of period recovery to be established to a reasonable degree including in the face of varying SNR levels and simulated flares. However the models were "too good" for equivalent width whilst "not good enough" for peak ratios. The need for a more sophisticated 3D model with vertical motion is clear if the activity in Proxima Centauri, probably other late M-dwarfs with lower rotation period but relatively high activity, are to be understood. It seems likely, however, that these methods will be of value for analysing spectra of faster rotating stars.

It was clear from the studies in Section 3.6 that many more observations, approaching the numbers from ASAS, are necessary to express confidence in periodicity results. On the other hand,

it was also clear from the modelling that signal to noise ratios down to about 20 do not disturb the results appreciably, even in the presence of flares.

In this process, however, as well as establishing the rotation period of Proxima Centauri with a reasonable degree of confidence, a recent alternative assessment of the rotation period as 116.6 days was clearly discounted as a false positive.

Appendix A

File formats

The software developed uses the following file formats.

A.1 Spectral Information File

The spectral information file, `specinfo`, is an XML file used to record the directory in which spectral observations are held and collate continuum normalisation, details of ranges, etc.

A selection of software was developed to manipulate these files, including in particular **Sdadmin**, which provides for interactive adjustment of the ranges.

A.2 Equivalent Width Files

The software developed for processing Equivalent Widths and Peak Ratios uses an 8-column file format with the following fields in each row.

1. Observation date, the Julian Date of the observation.
2. Barycentric Julian date of the observation. (In the case of models, this is a duplicate of column 1).
3. Equivalent Width, as calculated.
4. Calculated error on Equivalent Width.

5. (Now unused) a former measure, abandoned, called “Peak Size”.

6. Error on previous column.

7. Peak Ratio as calculated.

8. Calculated error on Peak Ratio.

“Short-cut” options to some of the software take arguments `--type ew` or `--type pr` to select the columns for Equivalent Width or Peak Ratio respectively[1].

[1] Plus `--type ps` to select the now unused column

Appendix B

Sdadmin program

The **Sdadmin** program is an interactive tool created to administer *Specinfo files*, as described in Section A.1, mainly to facilitate optimum GUI selection of ranges.

In the range selection facility, one or more spectra can be selected and simultaneously displayed on the range display window as illustrated in Fig. B.1 and ranges selected and adjusted using the control dialog as displayed in Fig. B.2. The range display is re displayed immediately to reflect the changes.

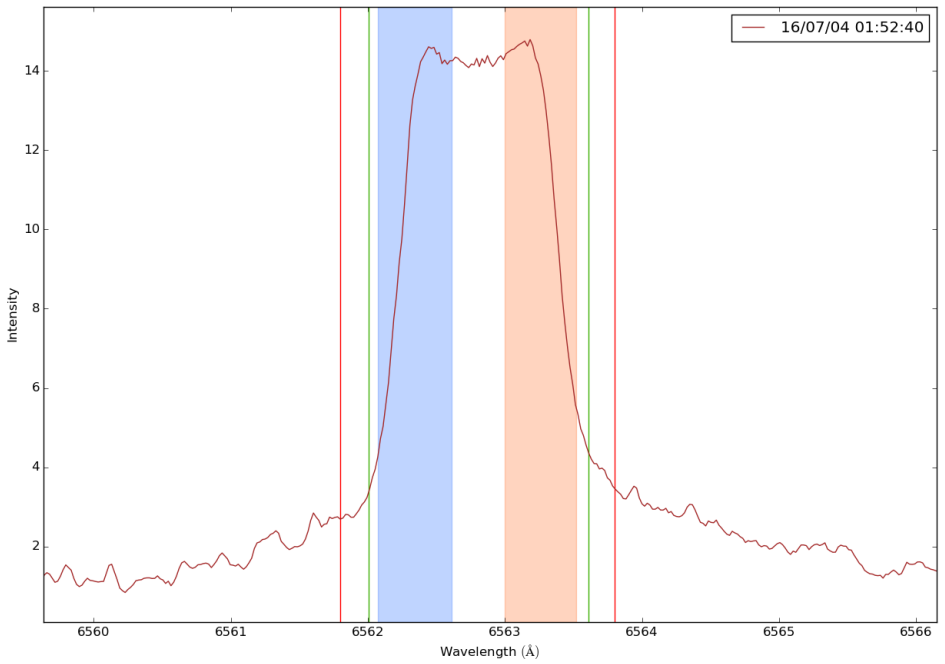

FIGURE B.1: The display window of the **Sdadmin** range selection option showing a Proxima Centauri spectrum from HARPS in the Hα region and with various ranges marked in.

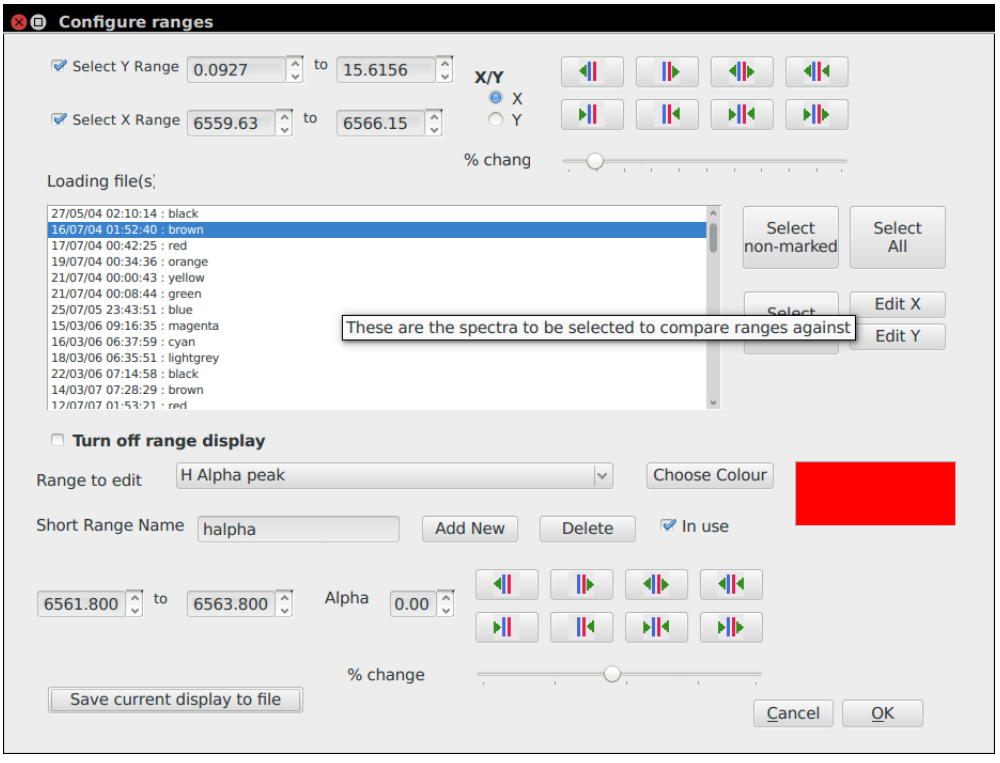

FIGURE B.2: The dialog window of the **Sdadmin** range selection option showing the facilities for adjusting the ranges and their display. Each element of the dialog has a popup help message as illustrated.

Appendix C

Lomb-Scargle Routines

A selection of Lomb-Scargle routines were employed to process the data in this report as no single routine provided all the facilities needed. As many of the processes undertaken were repetitive, routines which could operate in "batch" mode were required. This ruled out using Systemic[1], for example, which has a GUI interface.

C.1 Numerical Recipes

The Lomb-Scargle routine in the *Numerical Recipes* routines[2] was valuable in that it generates False Alarm Probabilities. The routine was enhanced for this report to extend to all the peaks found rather than just the maximum peak.

The main benefit with *Numerical Recipes* is that with this routine clear False Alarm Probabilities may be calculated, but a drawback is that there is comparatively little control over the periods examined. Some tuning of the oversampling factor and the maximum multiple of the Nyquist frequency may enable periods of interest to be recovered, but for many of the spectrographic datasets studied in this report such as the HARPS ones in Section 3.5 there are dominant apparent periods of 2 days or less which swamp the results and which the routine homes in upon. Sometimes a careful choice of binning can improve this, but at the cost of losing too many data points.

[1] Obtainable from http://www.stefanom.org

[2] This can be obtained from http://numerical-recipes/ in C and Fortran

However in the case of the photometric results in Chapter 2 the predominant peaks, found by this routine, are the ones of interest and a good estimate of the FAP is returned.

C.2 Scipy, AstroML, Gatspy

Also used were the Python Lomb-Scargle routines provided by SCIPY library (Jones et al., 2001), the ASTROML library, (Vanderplas et al., 2012) and the GATSPY library, (VanderPlas and Ivezić, 2015) and incorporated into Python software.

The main benefit of these routines is that the periods to be considered may be specified explicitly. However the drawback is no FAP is calculated.

If was found that with the photometric results in Chapter 2 where the *Numerical Recipes* routines gave a clear result and low FAP found, these routines returned identical results, but in the cases where the *Numerical Recipes* routines did not find the periods sought, such as for the photometric and modelling data, these routines all gave differing results. In a few cases the SCIPY library version gave division-by-zero errors and similar, hence the other two routines were generally preferred. However when the SCIPY library did work, the results tended to agree more with the GATSPY routine than the ASTROML routine, so in most cases the GATSPY routine was used.

C.3 Programs and usage

The *Numerical Recipes* program takes 5 arguments.

1. The input file which should be 2-column rows of time and intensity. The program **Colselect** may be used to select the required columns from a multi-column file.
2. The output file in 3 columns, period, power and FAP.
3. The oversampling factor, a float.
4. The highest multiple of the Nyquist frequency, a float.
5. A scaling factor, usually 1.0, which may be applied increase or reduce the differences between the times and then adjust the results. In some cases this can cause better results to be produced.

The SCIPY, ASTROML and GATSPY programs, **Lspfind**, **Alspfind** and **Glspfind** take a variety of keyword arguments of which the most important are:

`--period` Specifies the period range to search in the form start:interval:stop, for example `40d:.01d:130d`. The values are specified as a floating-point number followed by `d` to denote days or `h` to denote hours. If this is not specified, then the environment variable `PERIODS` is interrogated for a string of similar format.

`--outfile` Specifies the output file as the three column format as for the *Numerical Recipes* routine.

`--icol` Specifies the column of the input file, numbered from zero, to use for the intensity value, defaulting to 1.

`--tcol` Specifies the column of the input file, numbered from zero, to use for the times, defaulting to 0.

A final argument specifies the input file.

Alternative versions of the programs, **Lsconv**, **Alsconv** and **Glsconv** are provided for quickly processing Equivalent Width result files described in A.2, taking the argument `--type` with value `EW` or `PR` to select the appropriate column[3].

C.4 Window functions

It was not possible to derive window functions directly from any of the Lomb-Scargle routines used, either the Python routines or *Numerical Recipes*. Putting a constant value as the intensity alongside the observation times failed, either zero results were reported or overflows generated.

Some window function results were obtained from a third-party modification to the *Numerical Recipes* routine. It also proved possible to obtain window functions from the Python routines by supplying "white noise" (a uniform, a Gaussian and a combination function were tried with similar results) as the intensity alongside the observation times, repeating the calculation a number of times and averaging the results. The results obtained were all consistent with each other and with those for *Numerical Recipes* routine.

[3] Together with `PS` to select the now unused column.

The window functions displayed in Figs. 2.2, 2.3, 2.8, 3.14 and 3.15 were calculated by using *Period04* to avoid doubt about the validity of these, although they appeared to be comparable in the range of periods in question, at least for the photometric data. *Period04* did give results for periods up to 1.3% different from the Lomb-Scargle routines for ASAS and HST and gave completely different results for the HARPS data, as illustrated in Fig. 3.14 and Fig. 3.15, hence this was not used elsewhere in this report.

Appendix D

TiO Line Measurements

A prominent absorption line consistent across the spectra was identified to be a TiO transition at 6572.468Å to 6573.288Å, highlighted as the dark green shading in the right panel of Fig. 3.2. This is enlarged in Fig. D.1. The equivalent widths of this line from the HARPS data and also a version of the peak ratios in the same manner as for Table 3.1. Results are shown in Table D.1. Attempts were made to derive periodograms in the same manner as for Hα but no clear-cut results were obtained.

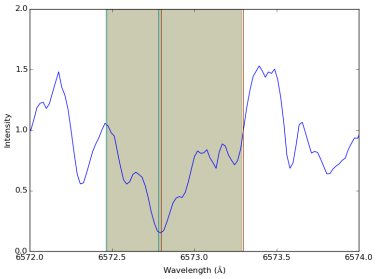

FIGURE D.1: This shows the section of the first spectrum in the HARPS data (at 27 May 2004 UTC 02:10:14) used for calculating Equivalent Widths and also Peak Ratios from the TiO absorption line from 6572.468Å to 6573.288Å. The blue vertical lines at 6572.463Å and 6572.784Å and the red lines at 6572.797Å and 6573.295Å delineate the regions used for calculation of a version of the Peak Ratios.

As Table D.1 shows, an "index" was also considered along the same lines as the Hα Index, but the size and variations (0.032 ± 0.001) were far too small to be useful.

From	To	No.	EW	Index	PR
27/05/2004	21/07/2004	6	0.309 ± 0.019	0.032 ± 0.002	1.039 ± 0.027
25/07/2005	22/03/2006	5	0.314 ± 0.004	0.032	1.017 ± 0.012
14/03/2007	19/07/2007	5	0.310 ± 0.006	0.032 ± 0.001	1.030 ± 0.036
29/06/2008	06/04/2010	25	0.315 ± 0.007	0.031 ± 0.001	1.020 ± 0.035
19/02/2011	03/06/2011	12	0.312 ± 0.008	0.032 ± 0.001	1.036 ± 0.024
18/01/2013	10/01/2014	207	0.310 ± 0.006	0.032 ± 0.001	1.047 ± 0.027
19/01/2016	30/03/2016	56	0.319 ± 0.015	0.031 ± 0.001	1.005 ± 0.028
ALL		316	0.312 ± 0.010	0.032 ± 0.001	1.036 ± 0.033

TABLE D.1: Results for calculation of median and standard deviation of the equivalent widths of the TiO transition at 6572.468Å to 6573.288Å from HARPS. The observations are separated where they are 300 or more days apart.

Bibliography

Anglada-Escudé, G., Amado, P.J., Barnes, J., et al., 2016. A terrestrial planet candidate in a temperate orbit around Proxima Centauri. *Nature*, 536:437.

Barnes, J.R., Jenkins, J.S., Jones, H.R.A., et al., 2012. Red Optical Planet Survey: a new search for habitable earths in the southern sky. *MNRAS*, 424:591.

Barnes, J.R., Jenkins, J.S., Jones, H.R.A., et al., 2013. Red Optical Planet Survey: A radial velocity search for low mass M dwarf planets. In *European Physical Journal Web of Conferences*, volume 47 of *European Physical Journal Web of Conferences*, page 5002.

Barnes, J.R., Jenkins, J.S., Jones, H.R.A., et al., 2014. Precision radial velocities of 15 M5-M9 dwarfs. *MNRAS*, 439:3094.

Benedict, G.F., McArthur, B., Nelan, E., et al., 1992. Hubble Space Telescope Astrometry and Photometry of Proxima Centauri using Fine Guidance Sensor #3. In *American Astronomical Society Meeting Abstracts*, volume 24 of *Bulletin of the American Astronomical Society*, page 1230.

Benedict, G.F., McArthur, B., Nelan, E., et al., 1998. Photometry of Proxima Centauri and Barnard's Star Using Hubble Space Telescope Fine Guidance Sensor 3: A Search for Periodic Variations. *AJ*, 116:429.

Benedict, G.F., Nelan, E., McArthur, B., et al., 1993. Periodic low-amplitude variations in the brightness of Proxima Centauri. *PASP*, 105:487.

Cincunegui, C., Díaz, R.F., and Mauas, P.J.D., 2007. A possible activity cycle in Proxima Centauri. *A&A*, 461:1107.

Claret, A., 2000. A new non-linear limb-darkening law for LTE stellar atmosphere models. *A&A*, 363:1081.

Collier-Cameron, A., 2001. *Astrotomography*. Lecture notes in Physics. Springer.

Dawson, R.I. and Fabrycky, D.C., 2010. Radial Velocity Planets De-aliased: A New, Short Period for Super-Earth 55 Cnc e. *ApJ*, 722:937.

Demory, B.O., Ségransan, D., Forveille, T., et al., 2009. Mass-radius relation of low and very low-mass stars revisited with the VLTI. *A&A*, 505:205.

Flores, M., González, J.F., Jaque Arancibia, M., et al., 2016. Discovery of an activity cycle in the solar-analog HD 45184. Exploring Balmer and metallic lines as activity proxy candidates. *ArXiv e-prints*.

Fuhrmeister, B., Lalitha, S., Poppenhaeger, K., et al., 2011. Multi-wavelength observations of Proxima Centauri. *A&A*, 534:A133.

Fuhrmeister, B., Liefke, C., Schmitt, J.H.M.M., et al., 2008. Multiwavelength observations of a giant flare on CN Leonis. I. The chromosphere as seen in the optical spectra. *A&A*, 487:293.

Giguere, M.J., Fischer, D.A., Zhang, C.X.Y., et al., 2016. A Combined Spectroscopic and Photometric Stellar Activity Study of Epsilon Eridani. *ApJ*, 824:150.

Gomes da Silva, J., Santos, N.C., and Bonfils, X., 2011. Long-term Stellar Activity Variations of Stars from the HARPS M-dwarf Sample: Comparison Between Activity Indices. In C. Johns-Krull, M.K. Browning, and A.A. West, editors, *16th Cambridge Workshop on Cool Stars, Stellar Systems, and the Sun*, volume 448 of *Astronomical Society of the Pacific Conference Series*, page 1117.

Guinan, E.F. and Morgan, N.D., 1996. Proxima Centauri: rotation, chromospheric activity, and flares. In *Bulletin of the American Astronomical Society*, volume 28 of *Bulletin of the American Astronomical Society*, page 942.

Guttenbrunner, S., Hanslmeier, A., Utz, D., et al., 2014. Solar Ca II K plage regions as proxies for magnetic fields of solar like stars. *Central European Astrophysical Bulletin*, 38:81.

Hall, J.C., 2008. Stellar Chromospheric Activity. *Living Reviews in Solar Physics*, 5.

Hall, J.C. and Lockwood, G.W., 1999. Evaluation of Solar Activity in Multiple Spectral Lines, 1994-1998. In *American Astronomical Society Meeting Abstracts*, volume 31 of *Bulletin of the American Astronomical Society*, page 1531.

Hall, J.C. and Lockwood, G.W., 2000. Composite Spectral Indices: A New Method for the Interpretation of Solar and Stellar Activity. *ApJ*, 541:436.

Hatzes, A.P., 2016. Periodic Hα variations in GL 581: Further evidence for an activity origin to GL 581d. *A&A*, 585:A144.

Jenkins, J.S., Ramsey, L.W., Jones, H.R.A., et al., 2009. Rotational Velocities for M Dwarfs. *ApJ*, 704:975.

Johnson, J.A., Butler, R.P., Marcy, G.W., et al., 2007. A New Planet around an M Dwarf: Revealing a Correlation between Exoplanets and Stellar Mass. *ApJ*, 670:833.

Jones, E., Oliphant, T., Peterson, P., et al., 2001. SciPy: Open source scientific tools for Python.

Kiraga, M. and Stepien, K., 2007. Age-Rotation-Activity Relations for M Dwarf Stars. *Acta Astron.*, 57:149.

Kitchatinov, L.L., Moss, D., and Sokoloff, D., 2014. Magnetic fields in fully convective M-dwarfs: oscillatory dynamos versus bistability. *MNRAS*, 442:L1.

Kneer, F., 2010. Chromosphere of active regions on the Sun . *MemSAI*, 81:604.

Kuridze, D., Mathioudakis, M., Jess, D.B., et al., 2011. Small-scale Hα jets in the solar chromosphere. *A&A*, 533:A76.

Kürster, M., Hatzes, A.P., Cochran, W.D., et al., 1999. Precise radial velocities of Proxima Centauri. Strong constraints on a substellar companion. *A&A*, 344:L5.

Linsky, J.L., Pagano, I., Valenti, J.A., et al., 2004. The Sun as a Star: Comparing Alpha Cen A to UV Solar Spectra. In A.K. Dupree and A.O. Benz, editors, *Stars as Suns : Activity, Evolution and Planets*, volume 219 of *IAU Symposium*, page 431.

Mohanty, S. and Basri, G., 2003. Rotation and Activity in Mid-M to L Field Dwarfs. *ApJ*, 583:451.

Mohanty, S., Basri, G., Shu, F., et al., 2002. Activity in Very Cool Stars: Magnetic Dissipation in Late M and L Dwarf Atmospheres. *ApJ*, 571:469.

Morin, J., Donati, J.F., Petit, P., et al., 2011. Exploring the magnetic topologies of cool stars. In D. Prasad Choudhary and K.G. Strassmeier, editors, *Physics of Sun and Star Spots*, volume 273 of *IAU Symposium*, pages 181–187.

Pojmanski, G., 1997. The All Sky Automated Survey. *Acta Astron.*, 47:467.

Pojmański, G., 2001. The All Sky Automated Survey (ASAS-3) System - Its Operation and Preliminary Data. In B. Paczynski, W.P. Chen, and C. Lemme, editors, *IAU Colloq. 183: Small Telescope Astronomy on Global Scales*, volume 246 of *Astronomical Society of the Pacific Conference Series*, page 53.

Rauscher, E. and Marcy, G.W., 2006. Ca II H and K Chromospheric Emission Lines in Late-K and M Dwarfs. *PASP*, 118:617.

Reiners, A., 2009. Activity-induced radial velocity jitter in a flaring M dwarf. *A&A*, 498:853.

Reiners, A. and Basri, G., 2008. Chromospheric Activity, Rotation, and Rotational Braking in M and L Dwarfs. *ApJ*, 684:1390.

Reiners, A., Mrotzek, N., Lemke, U., et al., 2015. The IAG solar flux atlas: Accurate wavelengths and absolute convective blueshift in standard solar spectra. *ArXiv e-prints*.

Robertson, P. and Mahadevan, S., 2014. Disentangling Planets and Stellar Activity for Gliese 667C. *ApJ*, 793:L24.

Robertson, P., Mahadevan, S., Endl, M., et al., 2014. Stellar activity masquerading as planets in the habitable zone of the M dwarf Gliese 581. *Science*, 345:440.

Robertson, P., Mahadevan, S., Endl, M., et al., 2015a. Response to Comment on Stellar activity masquerading as planets in the habitable zone of the M dwarf Gliese 581. *Science*, 347:1080.

Robertson, P., Roy, A., and Mahadevan, S., 2015b. Stellar Activity Mimics a Habitable-zone Planet around Kapteyn's Star. *ApJ*, 805:L22.

Rosa-González, D., Terlevich, E., and Terlevich, R., 2002. An empirical calibration of star formation rate estimators. *MNRAS*, 332:283.

Schmidt, S.J., Hawley, S.L., West, A.A., et al., 2015. BOSS Ultracool Dwarfs. I. Colors and Magnetic Activity of M and L Dwarfs. *AJ*, 149:158.

Stassun, K.G., Hebb, L., Covey, K., et al., 2011. The M4 Transition: Toward a Comprehensive Understanding of the Transition into the Fully Convective Regime. In C. Johns-Krull, M.K. Browning, and A.A. West, editors, *16th Cambridge Workshop on Cool Stars, Stellar Systems, and the Sun*, volume 448 of *Astronomical Society of the Pacific Conference Series*, page 505.

Suárez Mascareño, A., Rebolo, R., González Hernández, J.I., et al., 2015. Rotation periods of late-type dwarf stars from time series high-resolution spectroscopy of chromospheric indicators. *MNRAS*, 452:2745.

Tuomi, M. and Anglada-Escudé, G., 2013. Up to four planets around the M dwarf GJ 163. Sensitivity of Bayesian planet detection criteria to prior choice. *A&A*, 556:A111.

Tuomi, M., Jones, H.R.A., Barnes, J.R., et al., 2014. Bayesian search for low-mass planets around nearby M dwarfs - estimates for occurrence rate based on global detectability statistics. *MNRAS*, 441:1545.

Uitenbroek, H., 2004. Observational Aspects of Waves in the Chromosphere. In H. Lacoste, editor, *SOHO 13 Waves, Oscillations and Small-Scale Transients Events in the Solar Atmosphere: Joint View from SOHO and TRACE*, volume 547 of *ESA Special Publication*, page 107.

Unruh, Y.C., Solanki, S.K., and Fligge, M., 1999. The spectral dependence of facular contrast and solar irradiance variations. *A&A*, 345:635.

van Dokkum, P.G. and Conroy, C., 2010. A substantial population of low-mass stars in luminous elliptical galaxies. *Nature*, 468:940.

Vanderplas, J., Connolly, A., Ivezić, Ž., et al., 2012. Introduction to astroML: Machine learning for astrophysics. In *Conference on Intelligent Data Understanding (CIDU)*, pages 47 –54.

VanderPlas, J.T. and Ivezić, v., 2015. Periodograms for Multiband Astronomical Time Series. *ApJ*, 812:18.

Vernazza, J.E., Avrett, E.H., and Loeser, R., 1981. Structure of the solar chromosphere. III - Models of the EUV brightness components of the quiet-sun. *ApJ*, 45:635.

Winters, J.G., Henry, T.J., Lurie, J.C., et al., 2015. The Solar Neighborhood. XXXV. Distances to 1404 m Dwarf Systems Within 25 pc in the Southern Sky. *AJ*, 149:5.